

# Galaxy gas flows inferred from a detailed, spatially resolved metal budget

F. Belfiore,<sup>1,2</sup> R. Maiolino<sup>1,2</sup> and M. Bothwell<sup>1,2</sup>

<sup>1</sup> *Kavli Institute for Cosmology, University of Cambridge, Madingley Road, CB3 0HA Cambridge, UK*

<sup>2</sup> *Cavendish Laboratory, University of Cambridge, 19 J. J. Thomson Avenue, Cambridge, CB3 0HE, UK*

3 December 2024

## ABSTRACT

We use the most extensive integral field spectroscopic map of a local galaxy, NGC 628, combined with gas and stellar mass surface density maps, to study the distribution of metals in this galaxy out to 3 effective radii ( $R_e$ ). At each galactocentric distance, we compute the metal budget and thus constrain the mass of metals lost. We find that in the disc about half of the metals have been lost throughout the lifetime of the galaxy. The fraction of metals lost is higher in the bulge ( $\sim 70\%$ ) and decreases towards the outer disc ( $\sim 3 R_e$ ). In contrast to studies based on the gas kinematics, which are only sensitive to ongoing outflow events, our metal budget analysis enables us to infer the average outflow rate during the galaxy lifetime. By using simple physically motivated models of chemical evolution we can fit the observed metal budget at most radii with an average outflow loading factor of order unity, thus clearly demonstrating the importance of outflows in the evolution of disc galaxies. The observed gas phase metallicity is higher than expected from the metal budget and suggests late-time accretion of enriched gas, likely raining onto the disc from the metal-enriched halo.

**Key words:** galaxies: abundances – galaxies: evolution – galaxies: fundamental parameters – galaxies: individual (NGC 628)

## 1 INTRODUCTION

Current models of galaxy evolution predict that star formation and consequent metal enrichment in galaxies are regulated by a combination of gas inflows and outflows. In this framework, the enrichment of the intergalactic medium (IGM) is mediated by metal-rich outflows produced by galactic winds, especially during the early, more active phases of galaxy evolution (Oppenheimer & Dave 2006; Scannapieco et al. 2006; Shen, Wadsley & Stinson 2010; Oppenheimer et al. 2012). Evidence for ongoing metal-enriched outflows has been obtained both through absorption line studies of quasars whose lines of sight cross the vicinity of nearby galaxies (Tumlinson et al. 2011, 2013; Werk et al. 2013; Bregman et al. 2013) and through direct imaging of outflowing ionised or neutral/molecular gas at low and high redshift (Heckman et al. 2000; Martin 2005; Veilleux, Cecil & Bland-Hawthorn 2005; Martin 2006; Tremonti, Moustakas & Diamond-Stanic 2007; Feruglio et al. 2010; Sturm et al. 2011; Cano-Díaz et al. 2012; Maiolino et al. 2012; Cicone et al. 2014; Cazzoli et al. 2014; Arribas et al. 2014; Cicone et al. 2015). However, these observations are only probing ongoing events. A global understanding of the effect of outflows on the cosmic star formation history and IGM enrichment is only possible if we can gain insight into gas flows

over the entire evolutionary history of galaxies. The content and distribution of metals in galaxies can provide such information.

Metals are produced by stellar nucleosynthesis and act as a fossil record of a galaxy’s star formation history and gas flows. Simple analytical models relating metal abundances to star formation rate (SFR) and gas flow rates have been presented by several authors (Erb 2008; Lilly et al. 2013; Dayal, Ferrara & Dunlop 2013; Peng & Maiolino 2014a; Ascasibar et al. 2014) with the aim of explaining the scaling relations observed in statistical samples of galaxies. More detailed chemical evolutionary models have been successfully exploited to reproduce the observed chemical abundances, gas content and SFR of the solar neighbourhood, the Milky Way or nearby disc galaxies (Colavitti et al. 2009; Marcon-Uchida, Matteucci & Costa 2010; Spitoni & Matteucci 2011).

The common aim of chemical evolutionary models is to use chemical abundances observed today to infer the gas flow history and star formation history of the system. For example, in order to reproduce the chemical abundances of the Milky Way, a two-stage inflow model is generally invoked. The bulge is assumed to have formed at early times during a first inflow phase, while the disc is assumed to form inside-out during a second inflow phase (Matteucci & Fran-

cois 1989; Boissier & Prantzos 1999). Full hydrodynamical simulations of disc galaxies generally agree with the inside-out disc formation model (Pilkington et al. 2012). Chemical abundances can also provide clues on the relative importance of additional evolutionary processes in galaxies, including stellar migration, gas flows within the disc and large scale galactic fountains.

Current large integral field spectroscopy (IFS) galaxy surveys (eg. CALIFA, Sánchez et al. 2012; SAMI, Croom et al. 2012; MaNGA Bundy et al. 2014) offer great potential for extending the study of resolved chemical abundances to much larger galaxy samples. Using optical IFS data, the chemical abundance of the interstellar medium (ISM) can be derived by analysing gas emission lines, while insight into the metallicity of the stellar population can be obtained using Lick indices, or applying spectral decomposition techniques (Sanchez-Blazquez et al. 2014; Cid Fernandes et al. 2011). The CALIFA survey has recently delivered important insights on the distribution of metals within star-forming galaxies, providing the strongest evidence so far for a universal gas phase abundance gradient (Sánchez et al. 2014) out to 2 effective radii ( $R_e$ ), as already suggested in previous work (Vila-Costas & Edmunds 1992; Bresolin et al. 2009; Bresolin, Kennicutt & Ryan-Weber 2012).

However, observations of resolved gas metallicity alone cannot be uniquely related to specific chemical evolutionary models and, unless measurements of the gas and stellar content are also available, the information provided by the gas metallicity is highly degenerate between inflows and outflows.

This work presents one of the first attempts to combine chemical abundances from IFS with gas mass measurements from millimetre/radio observations for a single galaxy (NGC 628) on the same spatial scales, along with stellar mass surface density and stellar metallicities. We are therefore able to constrain the metal budget both as a function of radius, and for the galaxy as a whole, out to  $3 R_e$ . Since we have access to information on radial gradients of the relevant physical quantities, we obtain an overall metal budget free from aperture effects, which affected previous work based on metallicities estimated from observations of galaxy central regions (for example from the SDSS galaxy sample, York et al. 2000; Abazajian et al. 2009).

Empirical studies of the metal budget in the  $z = 0$  Universe, presented by several authors, agree in concluding that the total mass of metals produced by galaxies cannot be accounted for by the metals observed in stars and the ISM (Pettini et al. 1999; Ferrara, Scannapieco & Bergeron 2005; Bouche et al. 2007; Peeples & Shankar 2011; Zahid et al. 2012; Peeples et al. 2014). Large amounts of metals (between 35% and 90%) must be residing in the intergalactic medium, but also in the diffuse halo gas and in the circumgalactic medium (CGM). Although recent observational efforts have led to a better characterisation of the metallicity of the gas in the hot halo phase (Tumlinson et al. 2011, 2013), a robust metal budget for these phases is still missing.

Cosmological hydrodynamical simulations which include chemical evolution in a self-consistent way generally agree with the empirical studies above, and highlight that the fraction of missing metals is strongly dependant of the sub-grid feedback prescription (Wiersma, Schaye & Theuns 2011; Pilkington et al. 2012).

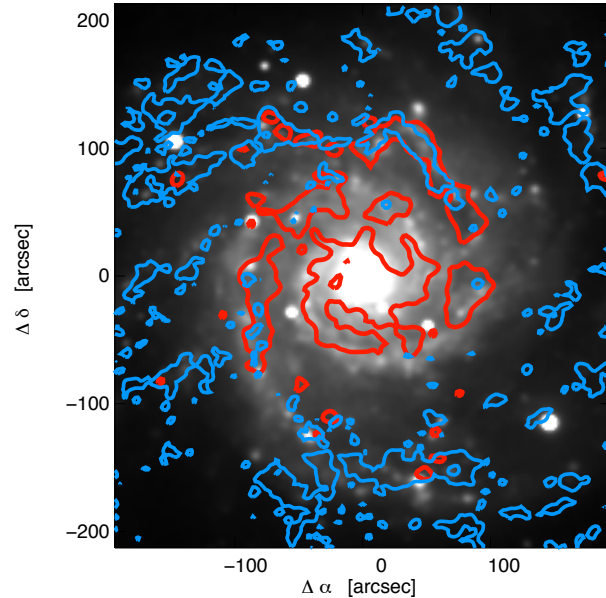


**Figure 1.** Optical image of NGC 628 ( $r'$  band from SDSS) with superimposed contours of HI (from the THINGS survey, in blue) and CO surface brightness (from the HERACLES survey, in red). The red contours correspond to a molecular hydrogen surface mass density of  $10 M_{\odot} \text{pc}^{-2}$ , while the blue HI contour correspond to a neutral hydrogen surface mass density of  $12 M_{\odot} \text{pc}^{-2}$ .

The aim of this work is to investigate in detail how metals are lost from the galaxy, hence the severity of the ‘missing metal problem’. This information also provides tight constraints on the outflow loading factor (i.e. the proportionality factor between SFR and outflow rate) *averaged* over the galaxy lifetime. The results are expected to provide simulators with new constraints on the net effect of gas flows in disc galaxies on resolved scales.

The paper is structured as follows. In Sec. 2 we give a brief overview of the observational data used, in Sec. 3 we summarise how we use the data to derive gas phase metallicity, gas and stellar mass surface densities and their radial gradients. In Sec. 4 we summarise the chemical evolution framework, while in Sec. 5 we present the results on the metal budget and the modelling of the outflow loading factor in NGC 628. In Sec. 6 and 7 we present the discussion and conclusions.

## 2 OVERVIEW OF THE DATA

NGC 628 is a nearby ( $D \approx 7.3 \text{ Mpc}$ ,  $z = 0.00219$ ) nearly face-on ( $i \approx 7^\circ$ ) spiral galaxy (Fig. 1). Table 1 summarises some of its basic properties. NGC 628 is a good example of an isolated galaxy (no encounter in the last Gyr; see Kamphuis & Briggs 1992), displaying typical grand-design structure. The following sections describe the observations of NGC 628 that have been used in this work.

**Table 1.** General properties of NGC 628

Property	Value
Name	NGC 628, M 74, UGC 1149
RA	00 <sup>h</sup> 59 <sup>m</sup> 50.1 <sup>s</sup>
Dec	-07°34'41.0"
Type	SAC
Distance (adopted)	7.3 Mpc
i	7°
$R_{24}$	4.88' = 10.3 kpc
$R_e$	67" = 2.4 kpc
scale	36 pc arcsec <sup>-1</sup>

## 2.1 Integral field spectroscopy

In this study we make use of IFS observations of NGC 628 taken as part of the PINGS survey (Rosales-Ortega et al. 2010; Sanchez et al. 2011; Rosales-Ortega et al. 2011). The survey was carried out using the 3.5-m telescope at the Calar Alto observatory, with the Potsdam Multi-Aperture Spectrograph in PPAK mode (Kelz et al. 2006). The PPAK fibre bundle corresponds to a field of view of 75" × 65" and consists of 331 science fibres of 2.7" diameter packed in an hexagonal pattern, leading to a filling fraction of 65%.

The data covers the spectral range between 3700 Å - 7100 Å, with a spectral resolution of FWHM  $\sim$  8Å. Due to the large projected size of the galaxy (10.5' × 9.5') the data consists of a mosaic of observations taken on 6 different nights over a period of 3 years. The final size of the mosaic is of 6' × 7'. We estimate the PSF to have a FWHM of approximately 3".

## 2.2 HI 21 cm observations

We use observations of the 21 cm line from THINGS (The HI Nearby Galaxy Survey, Walter et al. 2008). This survey comprises 34 nearby galaxies observed with the VLA, at high spectral ( $< 5.3 \text{ km s}^{-1}$ ) and spatial resolution. NGC 628 was observed using the B, C and D configurations with a combined on-source integration time of  $\sim 10$  hr. We use the publicly available<sup>1</sup> 'robust' weighted map (the 'robust' weighting scheme is used to achieve a sensitivity close to natural weighting while preserving a resolution close to uniform weighting, see Walter et al. 2008 for details), which has a beam size of  $\approx 6''$  ( $B_{\min} = 5.57''$ ,  $B_{\text{maj}} = 6.8''$ ). The  $1\sigma$  noise per 2.6 km s<sup>-1</sup> channel is 0.66 mJy beam<sup>-1</sup>, corresponding to a sensitivity of  $\approx 0.5 M_{\odot} \text{ pc}^{-2}$ , sufficient to trace the atomic hydrogen in all regions where it constitutes the dominant component of the ISM.

## 2.3 CO(2 -1) observations

We use observation of the CO(2 -1) transition to infer the molecular gas content. Maps are obtained from the publicly available<sup>2</sup> HERA CO-Extragalactic Survey (HERACLES, Leroy et al. 2009). HERACLES is a survey of 18 nearby galaxies using the HERA multi-pixel receiver on the IRAM 30 m telescope, with 13" angular resolution and 2.6 km s<sup>-1</sup>

spectral resolution. The  $1\sigma$  sensitivity of the map is estimated to be  $\approx 3 M_{\odot} \text{ pc}^{-2}$  (with the Galactic conversion factor discussed in Sect.3).

## 2.4 Multi-Wavelength Photometric Data

In this work we use photometry in different bands to obtain a reliable estimate of the stellar mass surface density by performing full spectral energy distribution (SED) fitting. We collected observations from GALEX (Galaxy Evolution Explorer), 2MASS (Two Micron All Sky Survey) and the Spitzer Space Telescope IRAC camera. In the optical band, we make use of the photometry from SDSS Data Release 7. Table 2 summarises the basic properties of the dataset used and the relevant references.

## 3 DATA ANALYSIS

In this section we present the analysis performed on the reduced data to obtain gas phase metallicities, stellar mass surface density and gas mass surface density profiles. We also briefly discuss the adopted choice of gas phase metallicity calibrators (Sec. 3.2) and the radial gradients of the derived quantities (Sec. 3.5). Throughout the section we highlight potential sources of systematic error.

### 3.1 Emission line fluxes

We extract emission line fluxes in each spaxel from the IFS datacube following a very similar procedure to Belfiore et al. (2014). Here we give a brief overview of the main steps involved.

(i) For each spaxel, we fit a linear combination of single stellar population (SSP) templates, after correction for systemic velocity and instrumental dispersion, using Penalised Pixel Fitting (Cappellari & Emsellem 2004). In this work we used a grid of 29 SSP templates, generated by using Maraston & Stromback (2011) models based on the empirical STELIB spectral library (Le Borgne et al. 2003). A spectral region of 600 km s<sup>-1</sup> is masked around each emission line we wish to fit. Strong sky lines are also masked. We do not attempt to extract stellar population parameters from the SSP fits. Such a study has recently been carried out by Sanchez-Blazquez et al. (2014), and in Sec. 5.1 we make use of the stellar metallicity gradient derived in their work.

(ii) For each spaxel, we subtract the stellar population fit from the observed spectrum to obtain a pure emission line spectrum. This is then fitted with a set of Gaussian functions, one per emission line (using least-squares minimization). The doublets [OIII]λλ4959, 5007 and [NII]λλ6548, 6584 are set to have the same velocity and velocity dispersion and the ratio of their intensities is fixed to the theoretical one. We calculate emission line fluxes by integrating the flux under the fitted Gaussians.

(iii) We apply a signal to noise cut to the emission line maps generated above, imposing a S/N larger than 5 in H $\alpha$  and H $\beta$ . This threshold is intentionally high to exclude regions of diffuse emission (mainly inter-arm regions) where

<sup>1</sup> <http://www.mpia.de/THINGS/Data.html>

<sup>2</sup> <http://www.mpia-hd.mpg.de/HERACLES/Data.html>

**Table 2.** Multi-wavelength observations of NGC 628 used in this work to supplement the IFS mosaic from Rosales-Ortega et al. (2010).

Telescope	Filter/Receiver	$\lambda_{\text{eff}}$ [Å]	Bandwidth [Å]	PSF FWHM ["]	Reference
GALEX	FUV	1516	268	4.3	Morrissey et al. (2007)
	NUV	2267	732	5.3	"
SDSS	u'	3540	599	1.49	Abazajian et al. (2009)
	g'	4770	1379	1.34	"
	r'	6222	1382	1.16	"
	i'	7632	1535	1.03	"
	z'	9060	1370	1.13	"
2MASS	J	1.235 [ $\mu\text{m}$ ]	0.162 [ $\mu\text{m}$ ]	2.5	Skrutskie et al. (2006)
	H	1.662 [ $\mu\text{m}$ ]	0.251 [ $\mu\text{m}$ ]	2.5	"
	K <sub>s</sub>	2.159 [ $\mu\text{m}$ ]	0.262 [ $\mu\text{m}$ ]	2.5	"
Spitzer	IRAC1	3.550 [ $\mu\text{m}$ ]	0.75 [ $\mu\text{m}$ ]	1.66	Fazio et al. (2004)
	IRAC2	4.493 [ $\mu\text{m}$ ]	1.01 [ $\mu\text{m}$ ]	1.72	"
IRAM 30m CO (2-1)	HERA	$\nu = 230.54$ [GHz]		13	Leroy et al. (2009)
VLA H <sub>i</sub>		$\nu = 1420.40$ [MHz]		$5.57 \times 6.80$	Walter et al. (2008)

the H $\alpha$  emission might not be ascribed to bona-fide HII regions. We do not impose signal to noise cuts on individual oxygen lines to avoid possible metallicity biases, but we discard regions where both the [OII] and the [OIII] line are undetected.

(iv) We calculate the reddening from the Balmer decrement, by using the H $\alpha$ /H $\beta$  ratio and a Calzetti (2001) attenuation curve with  $R_V = 4.05$ . The theoretical value for the Balmer line ratio is taken from Osterbrock & Ferland (2006), assuming case B recombination (H $\alpha$ /H $\beta = 2.87$ ). We note that the use of extinction curve of Cardelli, Clayton & Mathis (1989) (or the modification by O'Donnell 1994) with  $R_V = 3.1$  yields very similar results for the 3600 Å to 7000 Å wavelength range considered in this work.

### 3.2 Gas phase metallicity

Reliably measuring the gas metallicity from emission lines ratios remains a difficult problem in observational astrophysics. Different line ratios ('diagnostics') and methods ('calibrations') have been developed for the task. However it is well-known that different calibrations, even when based on the same diagnostics, can give results differing by up to 0.6 dex (Kewley & Ellison 2008; López-Sánchez et al. 2012; Peña Guerrero, Peimbert & Peimbert 2012). It is beyond the scope of this work to resolve the abundance scale problem (but see recent advances towards a possible solution in Dopita et al. 2013; Pérez-Montero 2014; Blanc et al. 2015). Fixing the gas phase metallicity scale is, however, a key factor in determining the total metal budget. We therefore discuss some of the assumptions going into widely used metallicity calibrators and possible shortcomings of each.

The metallicity (i.e. the oxygen abundance  $12 + \log(n(\text{O})/n(\text{H}))$ , where  $n$  denotes number densities), can be calculated knowing the electron temperature, which can be derived from the ratio of the oxygen auroral line [OIII] $\lambda$ 4363 and another oxygen line, like [OIII] $\lambda$ 5007. This method (referred to as the T<sub>e</sub> method<sup>3</sup>) is generally considered one

of the most reliable, at least in the low metallicity regime (Pagel et al. 1992; Garnett 1992; Izotov et al. 2006). At high metallicities, however, the electron temperature decreases and the auroral line is generally undetected. Moreover, temperature fluctuations make the T<sub>e</sub> method unreliable at high metallicities (Stasinska 2005; Bresolin 2007). Due to the strong temperature dependence of the emissivity of the auroral lines, regions with higher than average temperature may dominate the line emission, hence biasing the metallicity measurements towards low values. Finally, there is growing evidence that the distribution of electron energies in HII regions does not follow a Boltzmann distribution (Binette et al. 2012; Nicholls et al. 2013), hence making the definition of temperature arguable, while it seems that a  $\kappa$ -distribution is more appropriate (Dopita et al. 2013).

Recombination lines can also be used to estimate the metallicity. These are almost insensitive to temperature, which makes them much less dependent on temperature fluctuations and on the specific distribution of electron energies. However, these lines are approximately 10<sup>4</sup> times fainter than H $\beta$ , which makes their detection possible only for bright sources on 8-meter class telescopes. Metallicities estimated from the recombination lines are systematically offset, by about 0.2 dex, compared to those measured with the T<sub>e</sub> method (Blanc et al. 2015). Some authors (Peimbert & Peimbert 2010; Peña Guerrero, Peimbert & Peimbert 2012) attribute this discrepancy to the presence of small temperature fluctuations within HII regions, which (as discussed above) would bias the observed auroral line fluxes towards the highest temperature, lower abundance regions.

Finally, several authors have calibrated strong nebular line ratios (making use of [OIII] $\lambda$ 4959, 5007, [OII] $\lambda$ 3727, [NII] $\lambda$ 6584, etc) as abundance diagnostics. While the intensity of these lines depends on several factors besides the metal abundance (ionization parameter, density, N/O ratio), calibrations take advantage of the fact that in the HII regions observed in the local

known systematic uncertainties in T<sub>e</sub>-measured metallicities, we feel that this designation is inappropriate

<sup>3</sup> Or sometimes as the 'direct method'. However, given the well-

Universe relations exist between some of these parameters. Strong line diagnostics can be calibrated against  $T_e$ -based metallicity measurements (Pilyugin, Vílchez & Thuan 2010; Pilyugin & Thuan 2005; Pettini & Pagel 2004), photoionisation models (Denicolo, Terlevich & Terlevich 2002; Tremonti et al. 2004; Kobulnicky & Kewley 2004), or a mixture of both (Nagao, Maiolino & Marconi 2006; Maiolino et al. 2008). Recently, Blanc et al. (2015) has shown that some (but not all) photoionisation model grids are able to reproduce the metallicities measured using recombination lines.

To take into account the systematic uncertainty introduced by the choice of metallicity calibration, in this work we use two independently derived calibrations.

(i) The calibration from Maiolino et al. (2008) (M08), which is based on photoionisation models (Kewley & Dopita 2002) in the high metallicity regime and anchored to  $T_e$ -based metallicity measurements in the low metallicity regime. While M08 provides calibrations for various strong line diagnostics, here we use only the calibration based on the R23 parameter,

$$R_{23} = ([\text{OII}]\lambda 3727 + [\text{OIII}]\lambda 4959 + [\text{OIII}]\lambda 5007)/H\beta.$$

In the context of this work we have re-calculated the parametrisation of the R23-metallicity relation using the same procedure in M08, but using a 5th order polynomial fit (M08 used a fourth order polynomial) to provide a better fit to the high-metallicity end of the relation between  $12 + \log(\text{O}/\text{H})$  and R23. Overall the M08 calibration gives similar abundances to those obtained using the calibration used by Tremonti et al. (2004) and the calibration of R23 presented by Kobulnicky & Kewley (2004). Since the R23 parameter is double-valued, we break the degeneracy by using the  $[\text{NII}]/[\text{OII}]$  ratio, concluding that all the regions in NGC 628 belong to the upper branch of R23. We note that the use of a calibration the recursively solves for both metallicity and the ionisation parameter (Kobulnicky & Kewley 2004) does not substantially alter the derived metallicities.

(ii) The calibration from Pettini & Pagel (2004) (PP04), based mostly on  $T_e$  measurements, using the O3N2 index:

$$\text{O3N2} = \log \frac{[\text{OIII}]\lambda 5007/H\beta}{[\text{NII}]\lambda 6584/H\alpha}$$

This calibration has the disadvantage of depending explicitly on the the nitrogen abundance, which does not necessarily scale in a unique way with the oxygen abundance (Pérez-Montero & Contini 2009; Pérez-Montero 2014; Belfiore et al. 2014), since nitrogen has both a primary and a secondary nucleosynthetic origin and is released into the ISM on longer timescales than oxygen.

It is also worth noting that we are (perhaps unduly) extending the PP04 calibration to super-solar metallicities. In the original work of Pettini & Pagel (2004), only two HII regions with super-solar metallicity and  $T_e$  measurements are presented, while the high-metallicity end of the calibration is fixed by considering a small number of regions with metallicities calculated using photoionisation models. Even in the most recent calibration of the O3N2 diagnostic, presented by Marino et al. (2013), only 5 HII regions with super-solar metallicity are included, which makes any attempt to ‘directly’ calibrate the relation between O3N2 and metallicity

in the super-solar regime subject to large extrapolation uncertainties.

We also note that the two adopted calibrations make different assumptions regarding dust depletion of oxygen. In the M08 calibration, an oxygen depletion factor of 0.22 dex is assumed (Kewley & Dopita 2002), while  $T_e$ -based calibrations do not correct for the amount of oxygen depleted onto dust. We follow Peimbert & Peimbert (2010) and Peña Guerrero, Peimbert & Peimbert (2012) and modify the metallicities obtained from both calibrations assuming a constant oxygen depletion factor of 0.1 dex. For the rest of this work we will use gas phase metallicity to refer to the overall oxygen abundance of the ISM (gas and dust), with the understanding that the dust is taken into account through a constant depletion factor. Altering the dust depletion by  $\pm 0.1$  dex does not substantially change any of our conclusions.

Since M08 and PP04 are representative of the two main classes of metallicity calibrators ( $T_e$ -based and photoionisation-model-based), alternative calibrations will not lead to metallicity estimates significantly higher than M08 or significantly lower than PP04. Interestingly, recent work from Croxall et al. (2013), who used far-IR lines to estimate metallicity in NGC 628, points towards oxygen abundances within the range bracketed by the M08 and PP04 calibrations. Additionally Berg et al. (2013) obtained direct  $T_e$  measurements of metallicity for 11 HII regions in NGC 628, which agree on average, though with large scatter, with the metallicities derived with the PP04 calibration. The reason for the large scatter in the  $T_e$ -derived metallicities is not clear, however the scatter is considerably reduced by estimating  $T_e$  using the sulphur auroral lines, instead of the oxygen ones (Binette et al. 2012; Berg et al. 2015).

Since metallicity diagnostics are only calibrated for star forming regions (classical HII regions), regions of galaxies where other types of ionisation (shocks, active galactic nuclei, evolved stars, etc) are dominant should be excluded. We use the standard ionisation diagnostic diagram (BPT diagram Baldwin, Phillips & Terlevich 1981; Veilleux & Osterbrock 1987; Kewley et al. 2001; Kauffmann et al. 2003) to identify galactic regions as star-forming and follow Belfiore et al. (2014) in discarding regions that lie above the Kewley et al. (2001) demarcation line in the  $[\text{OIII}]/H\beta$  vs  $[\text{SII}]/H\alpha$  diagnostic diagram. All of the discarded spaxels are found in the inter-arm regions and present LINER-like ionisation, which might be due to evolved hot stars dominating the ionisation budget in regions where no recent star formation has taken place (Yan & Blanton 2012; Belfiore et al. 2014). We note that such regions, not complying with the HII classification, are only 5% of the total, and their exclusion or inclusion does not affect our final results.

The resulting maps of gas phase metallicity for the M08 and PP04 calibrations are shown in Fig. 2. For reference, the photospheric solar oxygen abundance, as derived by Asplund et al. (2009), is  $12 + \log(\text{O}/\text{H}) = 8.69$ , or equivalently  $Z_{\odot}(\text{O}) = 0.00585$ . Note that we are referring to  $Z$  as the oxygen abundance by mass. The total metal content (fraction by mass of elements heavier than helium) in the Sun is 0.0142, as given in Asplund et al. (2009).

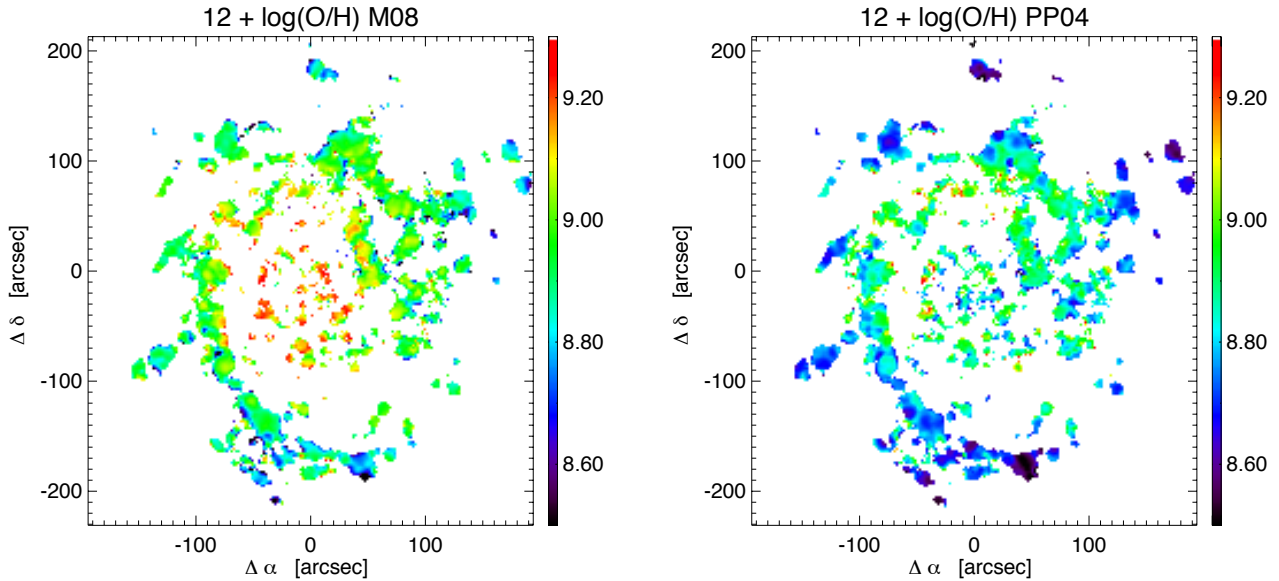


**Figure 2.** Maps of the gas metallicity in NGC 628 using the Maiolino et al. (2008) (M08) calibration based on R23 (left) and the Pettini & Pagel (2004) (PP04) calibration based on O3N2 (right). Only spaxels that lie below the Kewley et al. (2001) demarcation line in the [OIII]/H $\beta$  versus [SII]/H $\alpha$  BPT diagram are included.

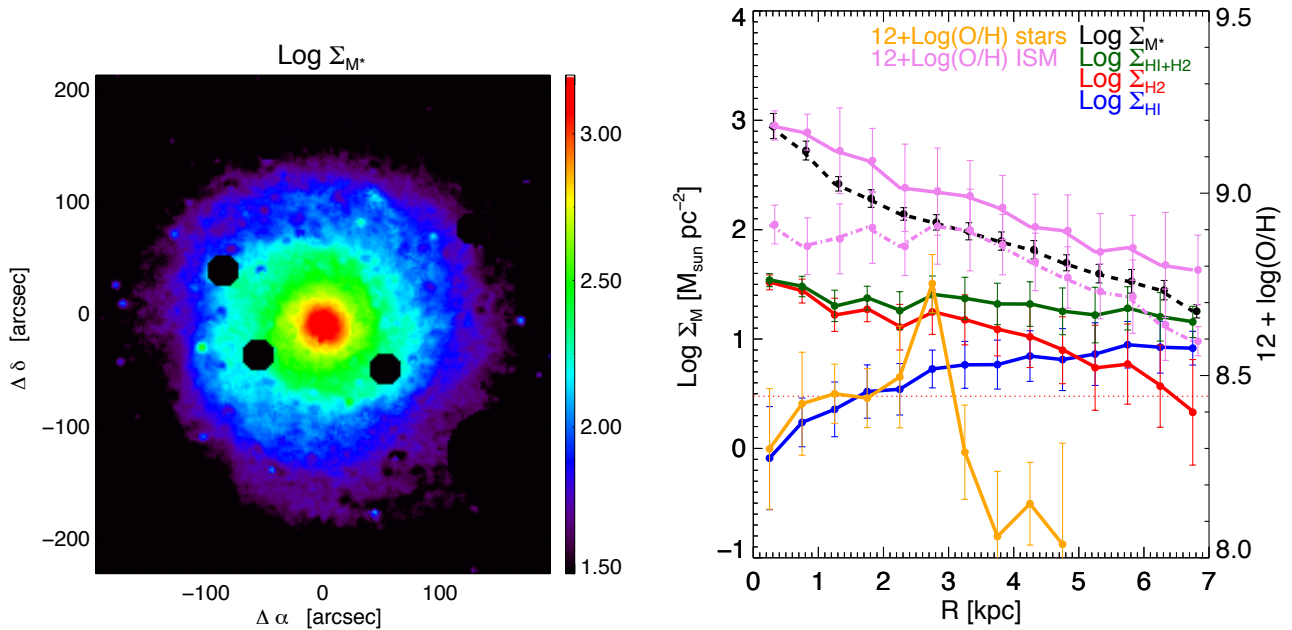


**Figure 3.** Left: Stellar mass surface density map, created from the spatially resolved SED fitting. Foreground stars have been masked. Right: Radial dependence of various physical quantities across the disk of NGC 628 (in radial bins; error bars represent the scatter in each radial bin). Atomic gas surface density (blue) shows a dip in the central region, while the molecular gas surface density (red) is peaked at the centre and quickly decreases outwards. The horizontal red dashed line corresponds to the sensitivity limit of the CO observations. The total gas content (green) is nearly flat across the whole disk up to  $3 R_e$  ( $1 R_e = 2.4 \text{ kpc}$ ). A clear radial gradient is observed in both stellar mass surface density (black, short dashes) and gas metallicity (violet). The latter is shown both for the M08 (solid violet) and PP04 (dot-dashed violet) metallicity calibrations. The stellar metallicity gradient from Sanchez-Blazquez et al. (2014) is shown in orange. Note that the metallicities of gas and stars are plotted with respect to the alternative y-axis on the right in units of  $12 + \log(\text{O}/\text{H})$ .

### 3.3 Stellar mass surface density

Stellar mass surface densities are estimated by performing SED fitting in each pixel on the multi-wavelength photometric data from UV to near IR, using the software package CIGALE (Code Investigating GALaxy Emission, Burgarella, Buat & Iglesias-Páramo 2005; Noll et al. 2009). In detail, we followed the procedure outlined below (similar to Boquien et al. 2012).

(i) The different observations were smoothed to the lowest resolution of the photometric dataset (GALEX NUV), using the kernels from Aniano et al. (2011).

(ii) The maps were then regridded on the same pixel scale as the IFS mosaic.

(iii) For each pixel, the flux and the flux error in each band was extracted. Errors are computed by taking into account the uncertainty in absolute calibration of the different instruments. Fluxes and errors are used as input for the software package CIGALE.

(iv) CIGALE creates FUV-to-FIR SEDs consisting of dust-attenuated complex stellar population models. In this analysis we used Maraston (2005) templates (with a Kroupa IMF) to build a grid of stellar models with a range in metallicity (from 0.5 to 2 solar). The star formation history is parametrised by an exponentially decreasing SFR, and an old stellar population with and a grid of younger stellar population bursts. Extinction is fitted using a Calzetti-like attenuation curve. The optimal galaxy parameters are derived by CIGALE using a Bayesian-like analysis. A map of stellar mass surface density is then created (Fig. 3, left panel)

The formal errors computed by CIGALE (which take into account the uncertainty in the data, but not the systematics of the method) are of the order of 0.1 dex. As a further check, we compared the stellar mass estimated by CIGALE with the stellar mass estimate obtained using the procedure in Bell et al. (2003) and using the u-r colour to estimate the mass-to-light ratio. The stellar mass densities obtained with the Bell formulation are totally consistent with the ones obtained with CIGALE, with a small systematic difference of less than 0.1 dex at very large radii ( $R > 8$  kpc). The total mass of NGC 628 out to  $3 R_e$  computed by CIGALE is  $\log(M_*/M_\odot) = 9.8$ .

### 3.4 Gas mass surface density

The HI mass can be calculated directly from the HI surface brightness, assuming that HI is everywhere optically thin.

To convert from CO luminosity to H<sub>2</sub> mass we adopt a constant CO to H<sub>2</sub> ( $\alpha_{CO}$ ) conversion factor given by

$$\alpha_{CO} = 4.35 \frac{M_\odot \text{ pc}^{-2}}{\text{K km s}^{-1}}$$

This value of the conversion factor is appropriate for the Milky Way (Solomon et al. 1987; Strong & Mattox 1996; Abdo et al. 2010; Bolatto, Wolfire & Leroy 2013). We explored the effect of using a metallicity-dependant conversion factor (Schruba et al. 2011) and the conversion factor derived by Blanc et al. (2009) by inverting the star-formation law in NGC 628, finding that none of our conclusions are substantially modified. As the conversion factors are cali-

brated for the CO (1-0) line, while the HERACLES observations map the CO (2-1) transition, we assume a constant ratio of 0.7 between the two CO luminosities (Leroy et al. 2012).

To calculate the total gas mass we multiply the HI component by 1.36 to account for helium and add the molecular gas mass computed using the conversion factor above, which already takes helium into account.

### 3.5 Radial gradients

It is well known that spiral galaxies exhibit radial gradients in their physical properties, including stellar mass surface density and metallicity (Bell & de Jong 2001; Moustakas et al. 2010; Delgado et al. 2013; Sánchez et al. 2014).

In Fig. 3 we present the radial gradients for the different physical quantities that we have derived in this section for NGC 628. We observe an exponential profile in stellar mass surface density and gas phase metallicity (black dashed and violet lines respectively). Intriguingly, both the stellar mass surface density and the metallicity gradient derived with the M08 calibration (solid violet line) have the same gradient within errors, leading to an almost linear  $\Sigma_* - Z$  relation. This is consistent with the analysis presented in Rosales-Ortega et al. (2012).

To take into account the metals locked in stars we make use of the recent study of Sanchez-Blazquez et al. (2014), who present the mass-weighted stellar metallicity gradient for NGC 628 by performing full spectral fitting using the software package STECKMAP on the same IFS data as used in this work. Taking into account the necessary correction factor due to the fact that Sanchez-Blazquez et al. (2014) adopt a different distance for NGC 628, we can obtain a stellar metallicity gradient out to 5 kpc. We put the gas phase and stellar metallicity on the same abundance scale by using the solar metallicity of Asplund et al. (2009) and assuming solar abundance ratios. We do not attempt to correct for possible non-solar abundance ratios (e.g.  $\alpha$ -enhancement) in the bulge, since in any case the correction will only affect our innermost radial bin and will not have a significant effect on the subsequent analysis of integrated properties.

We note here that the PP04 gas metallicity gradient presents a flattening in the inner 2.5 kpc ( $\approx 1 R_e$ , violet dot-dashed line), already reported in previous work (Rosales-Ortega et al. 2011) and consistent with the flattening observed in a subsample of galaxies from the CALIFA survey (Sánchez et al. 2014). With the current data it is not possible to assess whether this feature corresponds to a real abundance drop in the central region or if it is an artefact of the metallicity calibration. In particular, we note that such flattening observed when using the O3N2 calibration is often associated with a central decrease of the N/O abundance ratio (which can be traced by the [NII]/[OII] flux ratio), and this is also the case of NGC 628. Therefore the metallicity flattening may actually reflect a relative abundance variation affecting the metallicity diagnostic used in PP04, rather than a global metallicity flattening. However, we note that from the theoretical standpoint, bars and other non-axisymmetric perturbations can trigger large scale gas flows and induce a flattening of the metallicity gradient (Roskar et al. 2008a,b; Cavichia et al. 2013), together with a metallicity ‘hump’ at the interface. While the gas phase abundance does not

show evidence for this hump, a sharp increase in the stellar metallicity is reported at 2.5 kpc by Sanchez-Blazquez et al. (2014) (orange line in Fig. 3). They interpret this feature as the effect of an oval distortion (possibly a signature of a dissolving bar). The presence of a circum-nuclear ring of enhanced star formation seems to confirm this hypothesis.

The HI disc is much more extended than the FoV of the IFS data and presents clumpy substructure (seen in Fig. 1). The HI surface density profile is characterised by a central dip and an increase towards larger radii. The maximum in HI surface density coincides roughly with the edge of the IFS field of view ( $\approx 3 R_e$ ), hence in our subsequent analysis, which is limited to the radial extent of the IFS observations, we neglect about 40% of the mass of the HI disc. We will discuss the importance of this extended HI disc in Sec. 6.

The molecular gas profile is centrally concentrated and its surface density decreases with radius. The sensitivity limit of the HERACLES data is shown as a horizontal dotted line in Fig. 3. The combination of the atomic and molecular gas profile generates a total gas surface density profile (green line in Fig. 3) which is remarkably constant over the whole field of view of the IFS data. This implies that the gas fraction ( $f_{\text{gas}} = M_{\text{gas}}/(M_{\star} + M_{\text{gas}})$ ) increases outwards roughly log-linearly with radius.

#### 4 THE CHEMICAL EVOLUTION FRAMEWORK

In this section we present the analytical framework we will be using to study the metallicity evolution in resolved regions of NGC 628.

We make use of simple relations obtained by invoking the instantaneous recycling approximation and perfect instantaneous mixing. This framework has been proven successful in modelling the chemical evolution of oxygen (Zahid et al. 2012; Dayal, Ferrara & Dunlop 2013; Peebles et al. 2014; Peng & Maiolino 2014a), which is predominantly produced by short-lived massive stars dying as core-collapse supernovae. We note in passing that the chemical abundances of other common elements (like N or Fe) require a more detailed model, taking into account stellar lifetimes, the Type Ia supernovae delay time distribution and variation of the nucleosynthetic yields with metallicity, and will not be attempted in this work. However, since oxygen is the most abundant metal by mass, it is a good tracer for the total metal content.

Several studies in the literature have shown that, in order to interpret observed chemical abundances in galaxies, it is necessary to devise a model taking gas inflows and outflows into account (often dubbed the ‘gas regulatory model’) (Matteucci 1986; Gibson et al. 2003; Lilly et al. 2013; Dekel & Mandelker 2014; Peng & Maiolino 2014a).

Within the instantaneous recycling approximation, denoting the oxygen fraction (by mass) in the ISM as  $Z_g$ , the gas mass as  $M_g$ , the star formation rate as SFR, the stellar mass as  $M_{\star}$ , the total mass in oxygen in the galaxy as  $M_Z$ , the mass of oxygen in the ISM as  $M_{Zg}$ , the outflow rate as  $\Psi$  and the inflow rate as  $\Phi$ , the galaxy’s chemical evolution is described by the following equations

$$\frac{dM_g}{dt} = \Phi - (1 - R) \text{SFR} - \Psi, \quad (1)$$

$$\frac{dM_{\star}}{dt} = (1 - R) \text{SFR}, \quad (2)$$

$$\frac{dM_{Zg}}{dt} = \frac{d(M_g Z_g)}{dt} = y \text{SFR} - \Psi Z_g - (1 - R) Z_g \text{SFR}, \quad (3)$$

and

$$\frac{dM_Z}{dt} = y \text{SFR} - \Psi Z_g \quad (4)$$

where  $y$  is the mass of newly synthesised oxygen per unit mass of gas converted into stars (we will refer to it as the *net yield* per stellar generation) and  $R$  is the fraction of gas mass that is promptly returned to the ISM via stellar mass loss processes (referred to as the *return fraction*). We emphasise that the same relations apply also to the total abundance of metals (after replacing the appropriate value for the net nucleosynthetic yield), if the abundance ratios of different elements are assumed constant.

Both the average yield and the return fraction are a function of the initial mass function (IMF) and in general also depend on metallicity and time. In our simple model neither the time nor the metallicity dependence of  $R$  and  $y$  will be further considered, since the oxygen yield is shown to be approximately independent of metallicity and the effect of stellar lifetimes on the return fraction can be considered negligible for our purposes (Thomas, Greggio & Bender 1998; Kobayashi et al. 2006; Zahid et al. 2012, Vincenzo et al., in prep.).

If we denote as  $p(M)$  the net yield of oxygen for stars of mass  $M$ , then the net yield ( $y$ ) per stellar generation is given by

$$y = \frac{\int_{M_0}^{M_u} p(M) \text{IMF}(M) dM}{\int_{M_i}^{M_u} \text{IMF}(M) dM}, \quad (5)$$

where the  $\text{IMF}(M)$  is the initial mass function,  $M_i$  and  $M_u$  are the lower and upper mass cutoffs of the IMF, while  $M_0$  is the highest mass of the stars that are considered ‘eternal’ or, equivalently, the lowest mass of the stars contributing to the chemical enrichment. It is important to stress that the net yield ( $y$ ) is strongly dependent on the IMF, and not only on the ‘stellar’ nucleosynthetic yield  $p(M)$ . In fact, the average yield can vary by a factor larger than 3 for the same choice of stellar yields if the IMF is changed from Kroupa, Tout & Gilmore (1993) to Chabrier (2003) (Vincenzo et al, in prep.).

In this work, when a numerical value for the average yield is required, we make use of the yields of the most recent compilation of oxygen yield presented in Vincenzo et al. (in prep) which have been shown to successfully reproduce the oxygen abundance in the Milky Way (Romano et al. 2010). We adopt a Kroupa 1993 IMF (Kroupa, Tout & Gilmore 1993) and a lower mass cutoff  $M_0 = 1 M_{\odot}$  and therefore get a fiducial average yield of  $y = y_0 = 0.007$  for oxygen and  $R = 0.30$  (Vincenzo et al. in prep.). The same results can be applied to the *total* content of metals, by replacing the numerical value of the average yield with  $y = y_Z(\text{tot}) = 0.013$ .

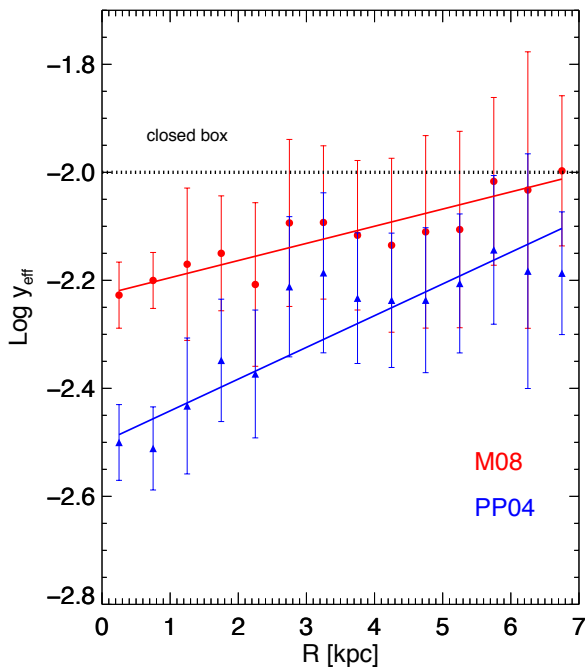


**Figure 4.** The radial variation of the effective yield in NGC 628. The value expected for the closed box case,  $y/(1-R) = 0.010$ , is indicated as a black dotted line. The red circles and blue triangles represent respectively the results obtained with the Maiolino et al. (2008) and Pettini & Pagel (2004) calibrations.

It can be easily shown that in the case of a ‘closed box’ evolution, i.e. no inflow and no outflow ( $\Phi = 0$  and  $\Psi = 0$ ), the gas metallicity is given by

$$Z_g = \frac{y}{1-R} \ln(f_g^{-1}), \quad (6)$$

where  $f_g = M_g/(M_g + M_*)$  is the gas fraction. Some authors find convenient to define the so-called ‘effective yield’ as

$$y_{\text{eff}} \equiv \frac{Z_g}{\ln(f_g^{-1})}. \quad (7)$$

Whenever  $y_{\text{eff}} \neq y/(1-R)$  Eq.6 implies that the system has not evolved as a closed box. Fig. 4 shows the radial gradient of the effective yield in NGC 628, clearly demonstrating that  $y_{\text{eff}}$  increases with radius. Importantly, the observed effective yield is always lower than  $y/(1-R) = 0.010$ , implying that the region of the disc of NGC 628 sampled by us has not been evolving as a closed box.

However, the information provided by the effective yield is highly degenerate. More specifically, both enriched gas outflows or pristine (or low metallicity) gas inflows will lead to the observed effective yield to be lower than the closed box value (Edmunds 1990).

## 5 RESULTS

### 5.1 A spatially resolved oxygen mass budget

The aim of this section is to compute the total mass of oxygen present in NGC 628 as a function of radius and compare it with the total mass of oxygen expected to have been produced by its stellar component.

This comparison provides a direct (model-independent) measurement of the mass of metals lost by each region in the galaxy via metal-enriched outflows. Moreover, the results obtained in this section can be directly compared with predictions from cosmological simulations.

Following Eq. 4, the total mass of oxygen *produced* is given by

$$M_{Z_{\text{prod}}} = \frac{y}{1-R} M_*. \quad (8)$$

This corresponds to the total mass of oxygen actually present in the galaxy in the case of no outflows (Eq. 4 with  $\Psi = 0$ ). The total observed mass of oxygen is given by the sum of the mass of oxygen in the ISM ( $M_{Z_g} = Z_g M_g$ ) and the mass of oxygen locked in stars ( $M_{Z_*} = Z_* M_*$ ), i.e.

$$M_{Z_{(\text{obs,tot})}} = M_{Z_g} + M_{Z_*} = Z_g M_g + Z_* M_*. \quad (9)$$

Both simulations (Marinacci et al. 2014) and observations (Shull, Smith & Danforth 2012; Tumlinson et al. 2013) argue that a large quantity of baryons and metals might reside in the hot haloes around galaxies. However, for the purposes of chemical evolution this gas is irrelevant since we assume it does not form stars, at least as long as it remains in the hot phase. Therefore in this work we consider this gaseous component as effectively external to the galaxy and the metals present in it as lost.

In Fig. 5 (left panel) we show the total observed mass of oxygen per unit area in stars (orange), in the ISM (violet), in ISM+stars (red) and the mass of metals that must have been produced by the observed stellar mass using our adopted yield (using Eq. 8, blue line) as a function of radius. In the case of the ISM and ISM+stars lines, we show the results obtained with both the M08 (solid) and PP04 (dashed) metallicity calibrations. The error bars represent the error in the mean in each annulus, added in quadrature to the median of the intrinsic error in each of the physical quantities. The intrinsic error budget is dominated by the error on the stellar metallicity, followed by the uncertainty in metallicity and stellar mass (for both we get a median error of about 0.1 dex). These errors do not attempt to incorporate systematic effects, which would dominate the uncertainty budget for this study. Moreover we take the net yield ( $y$ ) and the return fraction ( $R$ ) to be known exactly. With these caveats, Fig. 5 demonstrates that using the fiducial yield *at all radii more metals have been produced than can be accounted for considering both the metals in the ISM and in stars.*

In the discussion (Sec. 6) we argue that a different choice of IMF (adopting for example Salpeter or Chabrier IMF) only makes the metal deficit worse. We also note that the mass of metals in stars presents a sharp feature between 2.5 and 3 kpc, which is a direct consequence of the sharp feature in the stellar metallicity gradient. Since it is present in only one radial bin, the effect of this feature on the overall metal budget of the galaxy is negligible and will not be discussed further.

In Fig. 5, top right panel, we show the mass of oxygen in stars (orange) and ISM (violet) as a function of radius as a percentage of the total mass of oxygen produced in that annulus. The total mass of oxygen in each annulus (ISM + stars, red line) is also shown, and we plot the results using both the M08 (solid line) and PP04 (dot-dashed line) metallicity calibrations.

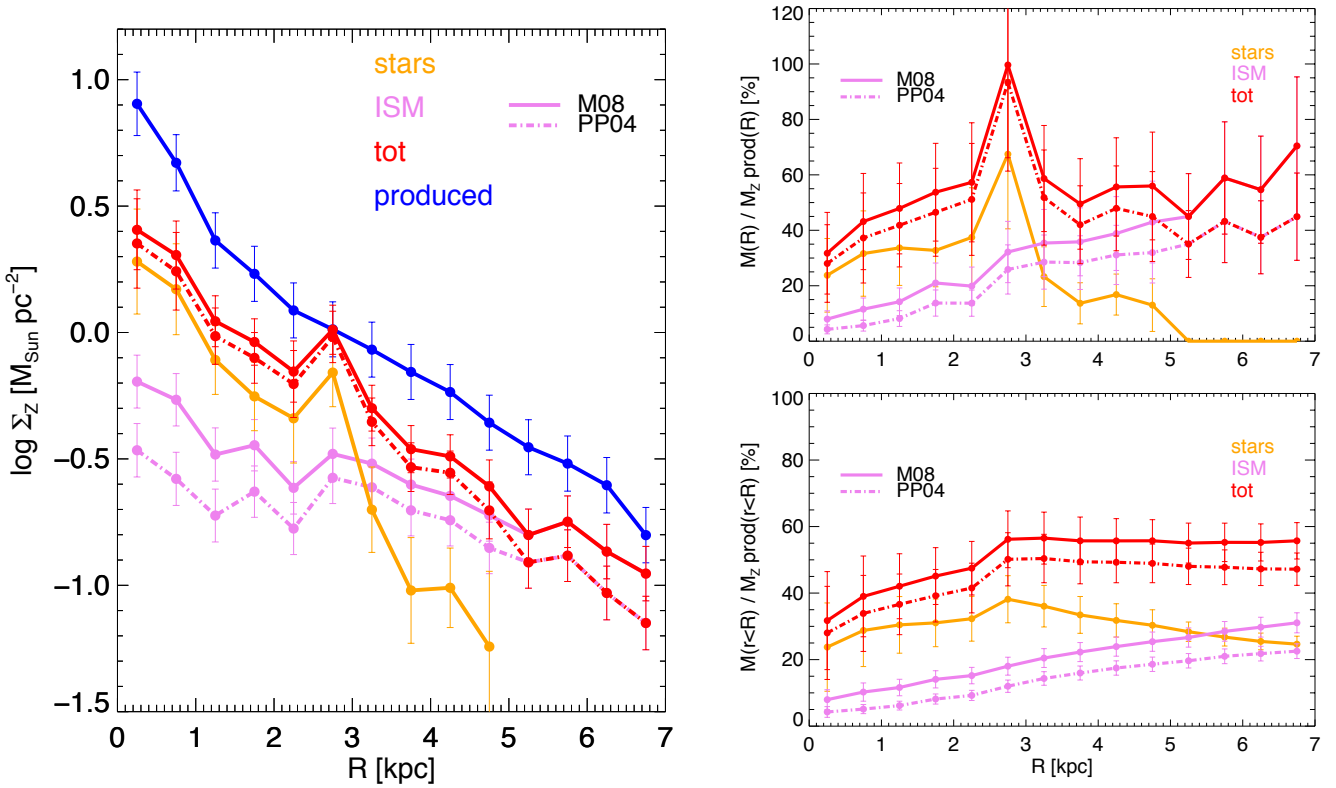


**Figure 5.** Left: Oxygen mass per unit area in different galactic components compared with the oxygen mass expected to have been produced by the observed stars, in different radial bins. The orange line shows the oxygen mass locked in stars, by using the stellar metallicity gradient from Sanchez-Blazquez et al. (2014). The violet solid line shows the oxygen mass in the ISM obtained by using the M08 calibration, while the violet-dashed line shows the oxygen mass in the ISM obtained by using the PP04 calibration. In red we show the total observed mass of oxygen (ISM + stars). The blue line shows the mass of oxygen produced by the stars at the same location assuming our fiducial average yield from Vincenzo (in prep.). Top Right: Mass of oxygen in each radial bin as a percentage of the mass of oxygen produced in the same radial bin. The colour-coding is the same as in the left panel. Bottom Right: The cumulative mass of oxygen within radius  $R$  in the different galactic component, expressed as a percentage of the total mass of oxygen produced within the same radius  $R$ . The points shown for the last radial bin correspond to the integrated oxygen budget for NGC 628, showing that the galaxy as a whole has retained only  $\approx 50\%$  of the metals it has produced.

Fig. 5 (top-right) shows that the fraction of metals lost is about 45%-55%, and approximately constant within the uncertainties for  $R > 3$  kpc. There is also some evidence that the fraction of metals lost in the central region is higher (only  $\sim 30\%$  of the metals have been retained). This feature may trace the effect of massive outflows during the formation of the bulge or the cumulative effect of AGN activity in the past. Interestingly Fig. 5 (top-right) also shows that the fraction of metals retained increases at  $R > 5$  kpc. Further gas phase metallicity measurements at even larger radii would be useful to confirm this trend.

Fig. 5 (lower-right) shows the *cumulative* version of the previous plot. For each radius  $R$ , the mass of oxygen in different components within radius  $R$  is computed as a percentage of the mass of metals produced within the considered radius. This plot can be interpreted as the results that would be obtained for the integrated properties of NGC 628 if all quantities (metallicities, gas masses etc) were measured using an aperture corresponding to radius  $a$   $R$  on the sky.

We note that cumulatively the mass of oxygen in the ISM is sub-dominant out to  $R \approx 5.5$  kpc, at the latter radius stars and ISM contribute roughly equally to the total oxygen budget. For easy reference, the masses of oxygen in

**Table 3.** The total oxygen mass in different galactic components, integrating the radial gradients out to  $R = 7.00$  kpc for NGC 628.

Metals	Mass [ $10^7 M_{\odot}$ ]	Mass [% $M_Z$ prod]
Stars	$2.6 \pm 0.9$	$25 \pm 2\%$
ISM (M08)	$3.2 \pm 0.9$	$31 \pm 3\%$
ISM (PP04)	$2.3 \pm 0.7$	$23 \pm 2\%$
Stars + ISM (M08)	$5.8 \pm 1.7$	$56 \pm 5\%$
Stars + ISM (PP04)	$4.9 \pm 1.5$	$47 \pm 5\%$

the different components within 7.0 kpc are summarised in Table 3. Taking into account the uncertainty associated with the choice of metallicity calibration, we conclude that out to  $R = 7.0$  kpc the bulge and the disc of NGC 628 as a whole have lost  $\sim 50\%$  of the oxygen they have produced.

## 5.2 Inferred net outflow loading factor

As discussed above, in the absence of outflows the total amount of metals produced should be simply given by the stellar mass times the amount of metals produced per stellar generation, i.e.  $t y / (1 - R)$  (Eq.8). To model the

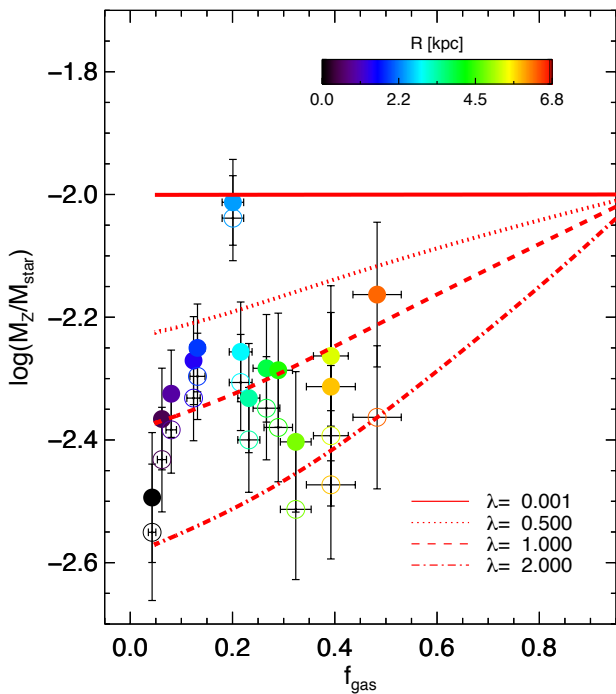


**Figure 6.** Metals-to-stellar mass ratio ( $M_Z/M_*$ ) versus gas fraction ( $f_{\text{gas}}$ ). Symbols show the values observed in radial annuli in NGC628, where the colour-coding gives the galactocentric radial distance, as indicated in the colourbar. Solid symbols correspond to the mass of metals in which the ISM metallicity is calculated by using the M08 calibration, while open symbols use the PP04 calibration. The red lines correspond to the prediction of simple chemical evolution models with different values for the average outflow loading factor  $\lambda$ . Note that the model relations are independent of the inflow rate  $\Phi$  and of the star formation efficiency  $\varepsilon$ .

effect of outflows we follow the formalism laid out in Peng & Maiolino (2014b) and assume the outflow rate  $\Psi$  to be proportional to the star formation rate through a constant outflow loading factor  $\lambda$ ,

$$\Psi = \lambda \text{SFR}. \quad (10)$$

The resulting total amount of metals is given by the equation

$$M_{Z(\text{tot})} = \frac{y}{1-R} M_* - \lambda \int Z_g(t) \text{SFR}(t) dt. \quad (11)$$

Evaluating the last term requires knowledge of the evolution of the metallicity with the star formation rate. To make further progress we therefore need to solve Eq. 1–2. A general solution as a function of time can be obtained assuming a star formation law. Following previous work we use a simple linear relation of the form

$$\text{SFR} = \varepsilon M_{\text{gas}} \quad (12)$$

where  $\varepsilon$  is often referred to as the *star formation efficiency* or also as the inverse of the gas depletion time ( $1/\tau_d$ ).

The final piece of information needed is the functional form of gas inflow rate  $\Phi$ . A number of authors have assumed a gas inflow rate proportional to the SFR (e.g. Matteucci & Chiosi 1983; Erb 2008; Mannucci et al. 2009; Dayal, Ferrara & Dunlop 2013; Troncoso et al. 2014; Kudritzki et al. 2015). This assumption leads to simple analytical solutions of the

resulting differential equations. Moreover it does not require consideration of the time variable, since all the quantities evolve in time like the SFR and hence the time dependence factors out. However, the assumption of an inflow rate proportional to the SFR has no physical grounds and has been used in previous work entirely for convenience. A much more realistic assumption is that of a constant, or slowly varying, inflow rate. As discussed in Peng & Maiolino (2014a) this assumption is much closer to the expectations for the inflow rate of baryons in dark halos expected in the cosmological framework and similar to what is inferred in numerical simulations of structure formation (Faucher-Giguère, Kereš & Ma 2011; Dekel et al. 2013).

Interestingly, analytical solutions of Equations 1–4 can still be obtained with the assumption of constant inflow rate, although they do depend explicitly on time. Exact solutions for  $M_g$  and  $M_*$  are given in Peng & Maiolino (2014a). Further exact solutions for  $Z_g$  and  $M_Z/M_*$  are presented in the Appendix. Here, we exploit those solutions to derive the relation between  $M_Z/M_{\text{star}}$  and the gas fraction.

We show in the Appendix that the exact relation between  $M_Z/M_*$  and  $f_{\text{gas}}$  is *independent* of both the inflow rate and of star formation efficiency and depends only on the outflow loading factor. This is a very important point, since the relation between these two quantities is therefore a clear, non-degenerate tracer of the net effect of outflows (unlike the effective yield). The red lines in Fig. 6 show  $M_Z/M_{\text{star}}$  as a function of  $f_{\text{gas}}$ , for different values of the outflow loading factor. Coloured symbols in Fig. 6 show the  $M_Z/M_{\text{star}}$  and  $f_{\text{gas}}$  observed in different radial annuli in NGC 628, where the colour coding represents the radial distance from the galaxy centre. Filled symbols are for the M08 calibration, while hollow symbols are for the PP04 calibration. We note that this figure is just an alternative representation of the metal deficit discussed in the previous section (Fig. 5), but here we have replaced the radial distance with  $f_{\text{gas}}$  as the x-axis and the metal deficit is given by the distance between the observational data point and the  $\lambda = 0$  (solid red) line.

By using the M08 calibration the observed points are well reproduced with an outflow loading factor  $\lambda \approx 1$ , with a scatter in the range  $0.5 < \lambda < 2$ , except for the ‘anomalous’ point at 3 kpc, which requires a lower loading factor approaching zero. The PP04 calibration requires slightly higher loading factors (except again for the anomalous point at 3 kpc).

We emphasise that, since we use the *total* mass of metals relative to the mass of stars, our analysis provides an estimate of the *average* outflow loading factor during the galaxy lifetime, and not the current outflow rate in the galaxy. Indeed, within the picture of hierarchical formation of structure, it is possible that this average loading factor is mainly driven by the high efficiency of metal loss at higher redshift, when the physical condition in the galaxy and its sub-components would have been significantly different.

Interestingly, a loading factor of  $\lambda \approx 1$  is in line with the value adopted by various cosmological simulations in order to reproduce the mass-metallicity relation and other galaxy parameter scaling relations (e.g. Davé, Finlator & Oppenheimer 2011). The higher loading factor associated with the central regions is possibly tracing the stronger outflow rate in the early phases of the rapid bulge formation and/or the

contribution of AGN-driven outflows during the lifetime of the galaxy.

### 5.3 Modelling the gas metallicity

As shown in the Appendix, the chemical evolution framework adopted in the previous section also leads to a direct relation between gas metallicity ( $Z_g$ ) and gas fraction ( $f_{\text{gas}}$ ) that depends only on the outflow loading factor and not on the inflow rate and star formation efficiency. The relation between  $Z_g$  and  $f_{\text{gas}}$  has been studied by several authors, including recently Ascasibar et al. (2014), who extend their analysis to resolved scales making use of data from NGC 628.

However, unlike the metals locked in stars, the gas phase metallicity is more subject to recent gas flow events, hence making it a less reliable tool for inferring the time averaged properties of the system.

Keeping these caveat in mind, the model relations between  $Z_{\text{gas}}$  and  $f_{\text{gas}}$  are shown in Fig. 7, with the same outflow loading factors as in Fig. 6. The data points represent the observed values in NGC 628 and are colour-coded by radial distance. The two different metallicity calibrations are identified, as in Fig. 6, by solid (Maiolino et al. 2008) and hollow (Pettini & Pagel 2004) circles. The comparison of the models with the data points suggests outflow loading factors consistent with zero, or generally much lower than those derived from the  $M_Z/M_{\text{star}}$  vs  $f_{\text{gas}}$  relation (Fig. 6).

We note that the mismatch applies (with about the same magnitude) both to the central regions, where the total mass of metals is dominated by the stellar component, and in the outer regions, where the total mass of metals is dominated by the gaseous component, therefore excluding that the mismatch is simply associated with a different metallicity scales or calibration issues associated with the calculation of one of the two quantities.

As discussed above, a possible solution can be attained assuming that the gas metallicity might not be representative of the average evolutionary processes during the life of the galaxy since it can be subject to recent galactic ‘weather’. In particular, a process that may strongly affect the gas metallicity, without significantly affecting the total content of metals, could be recent inflow of enriched gas from the halo. We discuss this option further in Sec. 6.

Finally we note that Kudritzki et al. (2015) have inferred a similarly low loading factor ( $\lambda = 0.2-0.3$ ) for NGC 628, by fitting the gas phase metallicity gradient and the gas fraction. Since they use  $T_e$ -based metallicities, their results should be compared with our analysis using the PP04 calibration, with which they are in qualitative agreement. However, Kudritzki et al. (2015) make use of a chemical evolution model where the inflow rate is proportional to the SFR. As discussed above, this assumption is not physically plausible and introduces a spurious dependence of the metallicity on the inflow rate, which is absent in our model.

## 6 DISCUSSION

In the previous section we have demonstrated that a) overall  $\sim 50\%$  of the oxygen produced by the NGC 628 out to  $R = 7.0$  kpc is unaccounted for and b) average outflow loading

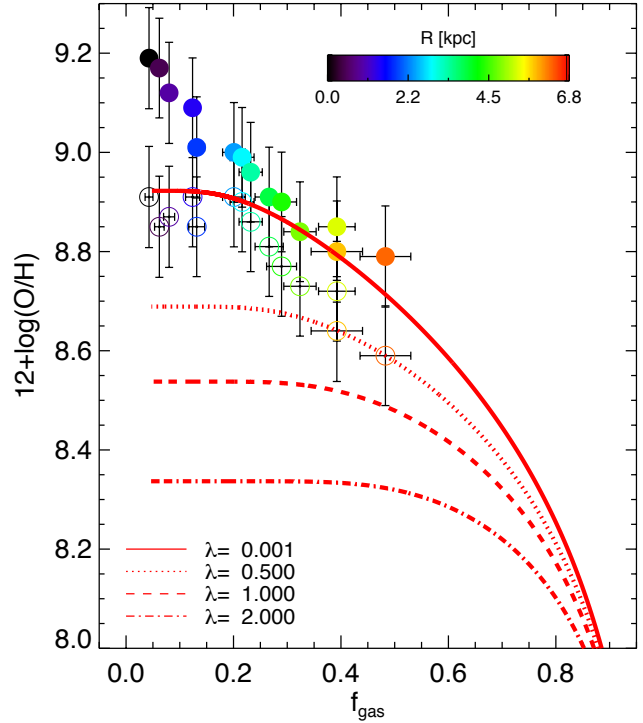


**Figure 7.** Gaseous metallicity  $12 + \log(\text{O}/\text{H})$  versus gas fraction. Symbols show the values observed in radial annuli in NGC 628, where the colour-coding gives the galactocentric radial distance, as indicated in the color-bar. Solid symbols correspond to the mass of metals in which the ISM metallicity is calculated by using the M08 calibration, while open symbols use the PP04 calibration. The red lines correspond to the prediction of simple chemical evolution models with different values for the average outflow loading factor ( $\lambda$ ). Note that the model relations are independent of the inflow rate  $\Phi$  and of the star formation efficiency  $\varepsilon$ .

factors of order unity can explain the observed metal deficit, although there is a tension with the observed gas metallicity. In this section we discuss possible ways to interpret these findings and future prospects to extend this work to more representative samples of galaxies.

### 6.1 Gas flows and disc-halo interaction

It is important to remember that the chemical evolution framework used in this work is an intentionally simple prescription. In particular, while the model allows metal rich outflows and pristine gas inflows, and hence some exchange of gas and metals between the different radial bins, it does not treat the case of incoming metal-rich gas or changes in the stellar mass component due to stellar migration.

A number of physical processes, for example, might be responsible for funnelling metal-rich gas into the central galactic regions, including viscous flows generated by gravitational instability or cloud - cloud collisions (Lacey & Fall 1985; Thon & Meusinger 1998; Ferguson & Clarke 2001) or the presence of a bar or other non-axisymmetric perturbation (Minchev & Famaey 2010; Matteo et al. 2013). The breaks seen in the stellar metallicity, and possibly the central flattening of the gas phase metallicity profile when using the PP04 calibration, combined with the presence of a star

formation ring just inside the break radius, may indeed support the hypothesis of an oval perturbation playing a role in the evolution of the disc in NGC 628.

More importantly, enriched gas expelled by previous generations of supernovae may fall back onto the disc, generating a galactic fountain. In the literature, however, there is no agreement on the details of the fountain mechanism (Melioli et al. 2008, 2009; Spitoni et al. 2010), the radial distance covered by a galactic fountain, the time needed for the gas to rain back onto the disc and the overall impact of this mechanism on the chemical abundances of the disc itself. In hydrodynamical simulations, if a hot halo is present, metal-enriched gas can fall back towards the galactic centre (Melioli et al. 2009). We have already argued in the previous section how the inflow of metal-rich gas from the halo might represent the most natural solution of the tension between metallicity and metal deficit.

The presence of large amounts of metals in the halo of disc (and elliptical) galaxies has been inferred by recent HST-COS observations of absorption systems along the line of sight of background quasars (e.g. Tumlinson et al. 2011; Werk et al. 2014). However, these observations have probed the halo of galaxies at large radii ( $\sim 100$  kpc). In the inner region of the halo the gas metallicity is not known observationally, but simulations expect that the metallicity of the diffuse gas should reach values higher than solar (Marinacci et al. 2014).

We have attempted to model an episode of metal-enriched accretion at late times by modifying the analytical description of the metallicity evolution discussed above with the introduction of an accreted enriched gas mass, proportional to the mass of baryons already present in the galaxy, and with a given metallicity  $Z_{\text{gas-accr}}$ . The blue lines in Fig. 8 shows the effect of such a late enriched accretion by assuming that the accreted gas is 1, 5 and 10% of the mass in baryons already present in the radial bin and that the metallicity of such enriched inflow is  $Z_{\text{gas-accr}} = 3 Z_{\odot}$  (which is consistent with the enrichment of the hot gas phase expected by models, Marinacci et al. 2014). Clearly such a model can now broadly reproduce the trend of the gas metallicities in NGC 628 at several radii. At the same time, Fig. 8 illustrates that such a late enriched accretion has little effect on the total content of metals, hence having little effect on the global, average outflow rate that we have inferred from the metal deficit.

In these models we have assumed an outflow loading factor  $\lambda = 2.0$ , i.e. higher than inferred in the previous section, to better illustrate that late enriched accretion can have a strong effect on the final gas metallicity but little effect on the total content of metals. We note that by starting with a lower loading factor (e.g.  $\lambda = 1.0$ ) the enriched inflow can reproduce the data with a smaller amount of accreted gas ( $\sim 3 - 5\%$ ).

Both gas flows in the disc and galactic fountains might therefore help resolve the tension between the metal deficit and the outflow loading factor implied from the gas phase metallicity for the central regions of NGC 628 by increasing the metallicity of the central regions beyond what is expected in the absence of these metal rich inflows.

Stellar migration (Roskar et al. 2008a; Joachim, Roškar & Debattista 2012; Spitoni et al. 2015) might also play a role in alleviating the observed tension. If stars diffuse out of the

radial bin in which they are born, we would be making incorrect inferences for the gas fraction and oxygen mass in the bin. We can model this effect naively by considering that the observed stellar mass in each bin should be corrected for the net effect of migration. We experimented with this prescription and found that changes in the stellar mass up to 0.3 dex only generate small changes in  $M_Z/M_*$  for all bins within  $R = 5$  kpc, since the metal budget is dominated by the stellar component and therefore  $M_Z/M_*$  is only weakly dependent on stellar mass. At larger radial distances the oxygen mass budget is dominated by the ISM and the effect of changing the stellar mass content is larger. If a large fraction of the stellar mass currently observed at large radii is the result of stellar migration from the centre, we would require a lower outflow loading factor in the outer disc, going towards a reduction of the tension between the metal deficit and the observed gas metallicity.

## 6.2 The oxygen deficit in context

Previous work has estimated the oxygen (or metal) budget in galaxies by statistical arguments, making use of scaling relations (between mass and SFR, between gas fraction and stellar mass, and between mass and metallicity) demonstrated to hold in large samples of galaxies observed spectroscopically (Bouche et al. 2007; Zahid et al. 2012; Peebles et al. 2014). These works predict an oxygen deficit ranging from 35% to 90%, with large statistical uncertainties, related both to the intrinsic scatter in the scaling relations used as input for the models and to the difficulty to robustly correct for aperture effects. Nonetheless it is rewarding to note that our estimate for the metal deficit in NGC 628 falls inside the range of estimates from previous works.

Due to the difficulty of studying the stellar metallicity and thus deriving the total metal content in galaxies, the relation between gas phase metallicity and gas fraction has been widely used as an observationally more accessible too to investigate the impact of outflows. However the discrepancy between the loading factors derived from the metal deficit and those derived from the gas phase metallicity, combined with the fact that gas phase metallicity is more sensitive to late-time gas mixing events, leads us to consider the outflow loading factors derived from the metal budget more reliable.

Extending this study to a larger sample of galaxies with resolved gas masses and metallicity information would provide the logical way forward to studying the effect of outflows across the whole galaxy population and uncover possible trends with galaxy parameters (stellar mass, SFR etc). While such a program is observationally costly, the synergy between large IFS surveys (CALIFA, SAMI and MaNGA) and radio and sub-mm interferometers (ALMA, NOEMA, JVLA) will greatly increase the availability of matched-resolution datasets to use for this type of study in the near future.

## 6.3 Towards larger galactocentric distances

The behaviour of the metal budget at even larger radii than the ones probed by our investigation constitutes a particularly interesting avenue for future work. Since HI discs ex-

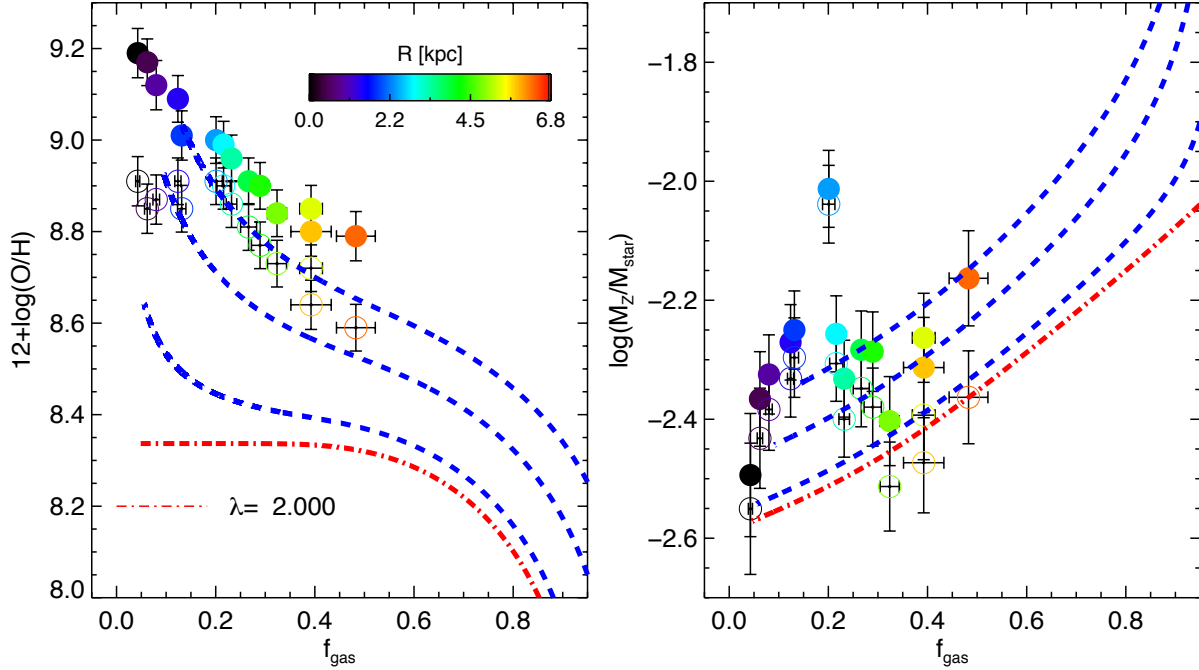


**Figure 8.** Same as Fig. 6 and 7, but including a late time inflow of gas rich material with metallicity  $3 Z_{\odot}$ . The red line is the same as in Fig. 6 and 7 and represents the model with  $\lambda = 2$ , while the blue lines represent an increasing mass of infalling metal-rich gas. Going upwards in both figures the blue lines represent an infalling metal-rich gas mass that is a fraction of 1%, 5% and 10% of the mass of baryons already present in the disc at a given location.

tend substantially more than the stellar component, low levels of chemical enrichment in the outer disc might mean that a large fraction of metals have escaped our budget. Unfortunately there is no consensus in the literature on the nature of the metallicity gradient for  $R > 2 R_e$ . While Bresolin, Kennicutt & Ryan-Weber (2012) and Sánchez et al. (2014) argue for a flattening of the gradient beyond  $R = 2 R_e$ , Moran et al. (2012) observed a sharp drop in the metallicity gradient for a subset of HI-rich galaxies.

Intriguingly, previous work has also presented evidence that HII regions at extreme galactocentric distances ( $R > R_{24} \approx 3 R_e$ ) are more metal rich than expected from in situ star formation (Bresolin et al. 2009; Bresolin, Kennicutt & Ryan-Weber 2012). These observations might be consistent with an extrapolation of the trend in Fig. 5, right panel, and in general with the idea that gas rich, relatively un-evolved systems have a smaller metal deficit. In the context of inside-out disc growth, these outer regions are still in the process of assembly and thus represent an ideal laboratory to study disc formation as it happens.

#### 6.4 The effect of the IMF

In this work we have used the Kroupa, Tout & Gilmore (1993) IMF, since this is the IMF which fits best the chemical evolution of galaxy discs (Romano et al. 2005, 2010). A different IMF would have an impact on our calculations, since different elements are produced by stars of different masses. In this section we briefly discuss the implications of adopting different IMFs.

A Salpeter IMF would give a significantly higher metal deficit, implying a loss of about 75% of the metals produced. The inferred average loading factor would be about  $\lambda \sim 2-4$ . In the case of a Chabrier (2003) IMF the metal deficit is even more severe: more than 85% of the metals should be lost and in the implied average loading factor should be in the range  $\lambda > 5$ . The Kroupa (2001) IMF gives results very similar to Chabrier (2003). We note that in going from a Kroupa to a Salpeter IMF we correct the stellar mass profile by a factor of 0.26 dex.

Such large loading factors are extreme, especially considering that these are loading factors averaged during the lifetime of the galaxy, and have never been seen in galactic winds studies locally or even in high- $z$  galaxy discs (e.g Steidel et al. 2010; Genzel et al. 2011), which instead infer outflow loading factors more in line with the results obtained by using the Kroupa, Tout & Gilmore (1993) IMF, further confirming that this IMF is the most appropriate for modelling galaxy discs.

However, it has been pointed out that the chemical properties of spheroids (including bulges) may be more properly described by a Chabrier (2003) IMF. So if we apply the latter IMF only to the central region, we get a large metal deficit ( $\sim 90\%$ ) for the bulge. This would be in line with a similar estimates for the Milky Way, according to which the bulge of our Galaxy has lost about 80% of its metals (Greggio & Renzini 2011). The Chabrier (2003) applied to the central region would also imply, as mentioned, a central outflow loading factor of about  $\lambda \sim 5$ . While such a large loading factor is unacceptably large for galaxy discs,

it might not be implausible for the central region of galaxies. Indeed outflow rates with such large loading factor are indeed seen in the central region of local and high- $z$  galaxies (Feruglio et al. 2010; Rupke & Veilleux 2011; Maiolino et al. 2012; Cicone et al. 2014, 2015), and may be explained with the additional boost to the outflow rate associated with quasar-driven winds or with extreme nuclear starbursts.

## 7 CONCLUSIONS

In this work we have presented a detailed study of the metal content and distribution in the nearby disc galaxy NGC 628. We have mapped the gas phase metallicity by exploiting the largest integral field spectroscopy mosaic available to date, thus enabling us to extend our study out to a galactocentric radius of 7 kpc ( $\sim 3 R_e$ ). We have combined the gas metallicity map with the stellar metallicity radial profile presented in previous work (Sanchez-Blazquez et al. 2014), the stellar mass surface density distribution  $\Sigma_*$  (inferred from extensive multi-band photometry) and the observed gas surface density ( $\Sigma_{\text{HI}}, \Sigma_{\text{H}_2}$ ) inferred from CO and HI maps.

By comparing the mass of metals observed in the gaseous and stellar components with the mass of metals produced by stars in the same region (inferred assuming the latest determination of the oxygen nucleosynthetic yield, Vincenzo et al., in prep.) we have obtained a detailed, spatially resolved metal budget as function of galactocentric radius. The main results from this analysis are the following:

(i) On average about 50% of the metals produced by the stars in each galactic region have been lost. The fraction of metals lost is higher ( $\sim 70\%$ ) in the central region, which is dominated by the bulge. This larger loss of metals relative to the rest of the disc may be associated with the larger outflow rate during the early formation of the bulge or with the cumulative effect of AGN-driven outflow events. There is also tentative indication that the fraction of metals lost decreases at large galactocentric radii. Cumulatively, out to a radius of 7 kpc, 45%–50% of the *total* amount of metals produced have been lost by the galaxy.

(ii) We have used simple (‘self-regulator’) analytical models involving gas outflow and inflow to model the data. In this framework the relation between metals-to-stellar mass ratio ( $M_Z/M_{\text{star}}$ ) and gas fraction ( $f_{\text{gas}}$ ) is independent of the inflow rate and of the efficiency of star formation, and depends only on the outflow loading factor. This removes many of the degeneracies plaguing previous studies and enables us to provide tight constraints on the outflow loading factor. We find that an outflow loading factor  $\lambda \approx 1$  can explain the data at most radii, though with large scatter ( $0.5 < \lambda < 2$ ). We emphasise that, since this inference is based on the total metal budget, we derive a time-averaged outflow rate, representative of the strength of outflows over the lifetime of the galaxy. This information is thus complementary to that obtained in studies based on the observed gas kinematics, which are sensitive only to the ongoing/recent outflow activity.

(iii) The gas phase metallicity is more sensitive to recent evolutionary processes because it is associated with a component of the galaxy (the ISM) that is potentially subject to rapid evolution. We find that the observed gas metallicity cannot be reproduced by the same parameters inferred from

the metal budget, independently from the choice of metallicity calibrator used. In particular, the observed gas phase metallicities would require little or no outflow. We show that the apparent tension can be most naturally explained with infall of enriched gas from the halo at late times. Indeed, such a process would strongly affect the observed gas metallicity, but not the total metal budget.

(iv) Finally, we warn against the use of analytical models in which the inflow rate is assumed to be proportional to the star formation rate. This assumption, adopted in previous work, is not physically motivated, may yield unphysical results and introduces spurious degeneracies between inflow and outflow rates. Analytical solutions are presented in this work for models assuming a constant, or slowly varying, accretion rate, which is a much better representation of gas inflows in the cosmological framework.

## ACKNOWLEDGMENT

This work makes use of THINGS (‘The Nearby Galaxy Survey’, Walter et al. 2008), HERACLES (the ‘HERA CO line Extragalactic Survey’, Leroy et al. 2009) and PINGS (the ‘PPAK IFS Nearby Galaxy Survey’, Rosales-Ortega et al. 2010). We thank Fiorenzo Vincenzo and Francesca Matteucci for their invaluable help in interpreting the vast literature on chemical abundance modelling and nucleosynthetic yields. We also thank Ying-jie Peng for support and discussion on development of his chemical evolution models. We wish to thank Fabian Rosales-Ortega for kindly sharing the PINGS data on NGC 628 and for his encouragement and feedback on the early stages of this work. We thank Matt Auger for useful discussions and healthy skepticism.

## REFERENCES

- Abazajian K. N. et al., 2009, *ApJS*, 182, 543
- Abdo A. A. et al., 2010, *ApJ*, 710, 133
- Aniano G., Draine B. T., Gordon K. D., Sandstrom K., 2011, *PASP*, 123, 1218
- Arribas S., Colina L., Bellocchi E., Maiolino R., Villar-Martin M., 2014, *A&A*, 568, A14
- Ascasibar Y., Gavil M., Pinto N., Casado J., Rosales F., 2014, *Arxiv*
- Asplund M., Grevesse N., Sauval a. J., Scott P., 2009, *ARA&A*, 47, 481
- Baldwin J. A., Phillips M. M., Terlevich R., 1981, *PASP*, 93, 5
- Belfiore F. et al., 2014, *ArXiv:1410.7781v1*
- Bell E. F., de Jong R. S., 2001, *ApJ*, 550, 212
- Bell E. F., McIntosh D. H., Katz N., Weinberg M. D., 2003, *ApJS*, 149, 289
- Berg D. A., Croxall K. V., Skillman E. D., Pogge R. W., Moustakas J., Groh-Johnson M., 2015, *ArXiv Prepr.*
- Berg D. a., Skillman E. D., Garnett D. R., Croxall K. V., Marble A. R., Smith J. D., Gordon K., Kennicutt R. C., 2013, *ApJ*, 775, 128
- Binette L., Matadamas R., Hägele G. F., Nicholls D. C., Magris G. C., 2012, *A&A*, 547, A29
- Blanc G. A., Heiderman A., Gebhardt K., Evans N. J., Adams J., 2009, *ApJ*, 704, 842

- Blanc G. a., Kewley L., Vogt F. P. a., Dopita M. a., 2015, *ApJ*, 798, 99
- Boissier S., Prantzos N., 1999, *MNRAS*, 307, 857
- Bolatto A. D., Wolfire M., Leroy A. K., 2013, *ARA&A*, 51, 207
- Boquien M. et al., 2012, *A&A*, 539, A145
- Bouche N., Lehnert M. D., Aguirre A., Peroux C., Bergeron J., 2007, *MNRAS*, 378, 525
- Bregman J. N., Miller E. D., Seitzer P., Cowley C. R., Miller M. J., 2013, *ApJ*, 766, 57
- Bresolin F., 2007, *ApJ*, 656, 186
- Bresolin F., Kennicutt R. C., Ryan-Weber E., 2012, *ApJ*, 750, 122
- Bresolin F., Ryan-Weber E., Kennicutt R. C., Goddard Q., 2009, *ApJ*, 695, 580
- Bundy K. et al., 2014, *ApJ*, 798, 7
- Burgarella D., Buat V., Iglesias-Páramo J., 2005, *MNRAS*, 360, 1413
- Calzetti D., 2001, *PASP*, 113, 1449
- Cano-Díaz M., Maiolino R., Marconi a., Netzer H., Shemmer O., Cresci G., 2012, *A&A*, 537, L8
- Cappellari M., Emsellem E., 2004, *PASP*, 116, 138
- Cardelli J. A., Clayton G. C., Mathis J. S., 1989, *ApJ*, 345, 245
- Cavichia O., Molla M., Costa R. D. D., Maciel W. J., 2013, *MNRAS*, 437, 3688
- Cazzoli S., Arribas S., Colina L., Bellocchi E., Emonts B., Maiolino R., 2014, *A&A*, 569, A14
- Chabrier G., 2003, *PASP*, 115, 763
- Cicone C. et al., 2015, *A&A*, 574, A14
- Cicone C. et al., 2014, *A&A*, 562, A21
- Cid Fernandes R., Stasiska G., Mateus a., Vale Asari N., 2011, *MNRAS*, 413, 1687
- Colavitti E., Cescutti G., Matteucci F., Murante G., 2009, *A&A*, 496, 429
- Croom S. M. et al., 2012, *MNRAS*, 421, 872
- Croxall K. V. et al., 2013, *ApJ*, 777, 96
- Davé R., Finlator K., Oppenheimer B. D., 2011, *MNRAS*, 421, 98
- Dayal P., Ferrara a., Dunlop J. S., 2013, *MNRAS*, 430, 2891
- Dekel A., Mandelker N., 2014, eprint arXiv:1402.2283, 2084, 2071
- Dekel a., Zolotov a., Tweed D., Cacciato M., Ceverino D., Primack J. R., 2013, *MNRAS*, 435, 999
- Delgado R. M. G. et al., 2013, *A&A*, 562, A47
- Denicolo G., Terlevich R., Terlevich E., 2002, *MNRAS*, 330, 69
- Dopita M. A., Sutherland R. S., Nicholls D. C., Kewley L. J., Vogt F. P. A., 2013, *ApJS*, 208, 10
- Edmunds M. G., 1990, *MNRAS*, 246, 678
- Erb D. K., 2008, *ApJ*, 674, 151
- Faucher-Giguère C. A., Kereš D., Ma C. P., 2011, *MNRAS*, 417, 2982
- Fazio G. G. et al., 2004, *ApJS*, 154, 10
- Ferguson a. M. N., Clarke C. J., 2001, *MNRAS*, 325, 781
- Ferrara A., Scannapieco E., Bergeron J., 2005, *ApJ*, 634, L37
- Feruglio C., Maiolino R., Piconcelli E., Menci N., Aussel H., Lamastra A., Fiore F., 2010, *A&A*, 518, L155
- Garnett D. R., 1992, *AJ*, 103, 1330
- Genzel R. et al., 2011, *ApJ*, 733, 101
- Gibson B. K., Fenner Y., Renda A., Kawata D., Lee H.-c., 2003, *PASA*, 401
- Greggio L., Renzini A., 2011, *Stellar Populations. A User Guide from Low to High Redshift*. Wiley-VCH Verlag GmbH & Co. KGaA
- Heckman T. M., Lehnert M. D., Strickland D. K., Armus L., 2000, *ApJS*, 129, 493
- Izotov Y. I., Stasiska G., Meynet G., Guseva N. G., Thuan T. X., 2006, *A&A*, 448, 955
- Kamphuis ., Briggs ., 1992, *A&A*, 253, 335
- Kauffmann G. et al., 2003, *MNRAS*, 346, 1055
- Kelz A. et al., 2006, *PASP*, 118, 129
- Kewley L. J., Dopita M. A., 2002, *ApJS*, 142, 35
- Kewley L. J., Dopita M. A., Sutherland R. S., Heisler C. A., Trevena J., 2001, *ApJ*, 556, 121
- Kewley L. J., Ellison S. L., 2008, *ApJ*, 681, 1183
- Kobayashi C., Umeda H., Nomoto K., Tominaga N., Ohkubo T., 2006, *ApJ*, 653, 1145
- Kobulnicky H. A., Kewley L. J., 2004, *ApJ*, 617, 240
- Kroupa P., 2001, *MNRAS*, 322, 231
- Kroupa P., Tout C. A., Gilmore G., 1993, *MNRAS*, 262, 545
- Kudritzki R.-P., Ho I.-T., Schrubba A., Burkert A., Zahid H. J., Bresolin F., Dima G. I., 2015, *ArXiv e-prints*
- Lacey C. G., Fall S. M., 1985, *ApJ*, 290, 154
- Le Borgne J.-F. et al., 2003, *A&A*, 402, 433
- Leroy A. K. et al., 2012, *AJ*, 144, 3
- Leroy A. K. et al., 2009, *AJ*, 137, 4670
- Lilly S. J., Carollo C. M., Pipino A., Renzini A., Peng Y., 2013, *ApJ*, 772, 119
- López-Sánchez A. R., Dopita M. A., Kewley L. J., Zahid H. J., Nicholls D. C., Scharwächter J., 2012, *MNRAS*, 426, 2630
- Maiolino R. et al., 2012, *Mon. Not. R. Astron. Soc. Lett.*, 425, L66
- Maiolino R. et al., 2008, *A&A*, 488, 463
- Mannucci F. et al., 2009, *MNRAS*, 398, 1915
- Maraston C., 2005, *MNRAS*, 362, 799
- Maraston C., Stromback G., 2011, *MNRAS*, 418, 2785
- Marcon-Uchida M. M., Matteucci F., Costa R. D. D., 2010, *A&A*, 520, A35
- Marinacci F., Pakmor R., Springel V., Simpson C. M., 2014, *MNRAS*, 442, 3745
- Marino R. A. et al., 2013, *A&A*, 559, A114
- Martin C. L., 2005, *ApJ*, 621, 227
- Martin C. L., 2006, *ApJ*, 647, 222
- Matteo P. D., Haywood M., Combes F., Semelin B., Snaith O. N., 2013, *A&A*, 553, A102
- Matteucci F., 1986, *PASP*, 98, 973
- Matteucci F., Chiosi C., 1983, *A&A*, 123, 121
- Matteucci F., Franco P., 1989, *MNRAS*, 239, 885
- Melioli C., Brighenti F., D’Ercole a., de Gouveia Dal Pino E. M., 2008, *MNRAS*, 388, 573
- Melioli C., Brighenti F., D’Ercole a., de Gouveia Dal Pino E. M., 2009, *MNRAS*, 399, 1089
- Minchev I., Famaey B., 2010, *ApJ*, 722, 112
- Moran S. M. et al., 2012, *ApJ*, 745, 66
- Morrissey P. et al., 2007, *ApJS*, 173, 682
- Moustakas J., Kennicutt R. C., Tremonti C. a., Dale D. a., Smith J.-D. T., Calzetti D., 2010, *ApJS*, 190, 233
- Nagao T., Maiolino R., Marconi A., 2006, *A&A*, 459, 85

- Nicholls D. C., Dopita M. A., Sutherland R. S., Kewley L. J., Palay E., 2013, *ApJS*, 207, 21
- Noll S., Burgarella D., Giovannoli E., Buat V., Marcellac D., Muñoz Mateos J. C., 2009, *A&A*, 507, 1793
- O'Donnell J. E., 1994, *ApJ*, 422, 158
- Oppenheimer B. D., Dave R., 2006, *MNRAS*, 373, 1265
- Oppenheimer B. D., Davé R., Katz N., Kollmeier J. a., Weinberg D. H., 2012, *MNRAS*, 420, 829
- Osterbrock D. E., Ferland G. J., 2006, *Astrophysics of gaseous nebulae and active galactic nuclei*. University Science Books, Mill Valley, CA
- Pagel B. E. J., Simonson E. A., Terlevich R. J., Edmunds M. G., 1992, *MNRAS*, 255, 325
- Peña Guerrero M. a., Peimbert A., Peimbert M., 2012, *ApJ*, 756, L14
- Peebles M. S., Shankar F., 2011, *MNRAS*, 417, 2962
- Peebles M. S., Werk J. K., Tumlinson J., Oppenheimer B. D., Prochaska J. X., Katz N., Weinberg D. H., 2014, *ApJ*, 786, 54
- Peimbert A., Peimbert M., 2010, *ApJ*, 724, 791
- Peng Y.-j., Maiolino R., 2014a, *MNRAS*, 443, 3643
- Peng Y.-j., Maiolino R., 2014b, *MNRAS*, 438, 262
- Pérez-Montero E., 2014, *ArXiv:1404.3936v2*
- Pérez-Montero E., Contini T., 2009, *MNRAS*, 398, 949
- Pettini M., Ellison S. L., Steidel C. C., Bowen D. V., 1999, *ApJ*, 510, 576
- Pettini M., Pagel B. E. J., 2004, *MNRAS*, 348, L59
- Pilkington K. et al., 2012, *A&A*, 540, A56
- Pilyugin L. S., Thuan T. X., 2005, *ApJ*, 631, 231
- Pilyugin L. S., Vílchez J. M., Thuan T. X., 2010, *ApJ*, 720, 1738
- Romano D., Chiappini C., Matteucci F., Tosi M., 2005, *A&A*, 430, 491
- Romano D., Karakas A. I., Tosi M., Matteucci F., 2010, *A&A*, 522, A32
- Rosales-Ortega F. F., Díaz a. I., Kennicutt R. C., Sánchez S. F., 2011, *MNRAS*, 415, 2439
- Rosales-Ortega F. F., Kennicutt R. C., Sánchez S. F., Díaz a. I., Pasquali A., Johnson B. D., Hao C. N., 2010, *MNRAS*, 405, 735
- Rosales-Ortega F. F., Sanchez S. F., Iglesias-Páramo J., Diaz A. I., Vilchez J. M., Bland-Hawthorn J., Mast D., 2012, *ApJ*, 756, L31
- Roskar R., Debattista V. P., Quinn T. R., Stinson G. S., Wadsley J., 2008a, *ApJ*, 684, L79
- Roskar R., Debattista V. P., Stinson G. S., Quinn T. R., Kaufmann T., Wadsley J., 2008b, *ApJ*, 675, L65
- Rupke D. S. N., Veilleux S., 2011, *Astrophys. J. Lett.*, 729, L27
- Sanchez S., Rosales-Ortega F., Kennicutt R. C., Johnson B. D., Diaz A. I., Pasquali A., Hao C. N., 2011, *MNRAS*, 410, 313
- Sánchez S. F. et al., 2012, *A&A*, 538, A8
- Sánchez S. F. et al., 2014, *A&A*, 563, A49
- Sanchez-Blazquez P., Rosales-Ortega F., Diaz A., Sanchez S. F., 2014, *MNRAS*, 437, 1534
- Scannapieco C., Tissera P. B., White S. D. M., Springel V., 2006, *MNRAS*, 371, 1125
- Schruba A. et al., 2011, *AJ*, 142, 37
- Shen S., Wadsley J., Stinson G., 2010, *MNRAS*, 407, 1581
- Shull J. M., Smith B. D., Danforth C. W., 2012, *ApJ*, 759, 23
- Skrutskie M. F. et al., 2006, *AJ*, 131, 1163
- Solomon P. M., Rivolo A. R., Barrett J., Yahil A., 1987, *ApJ*, 319, 730
- Spitoni E., Calura F., Matteucci F., Recchi S., 2010, *A&A*, 514, A73
- Spitoni E., Matteucci F., 2011, *A&A*, 531, A72
- Spitoni E., Romano D., Matteucci F., Ciotti L., 2015, *Arxiv Prepr.*
- Stasinska G., 2005, *A&A*, 434, 507
- Steidel C. C., Erb D. K., Shapley A. E., Pettini M., Reddy N., Bogosavljević M., Rudie G. C., Rakic O., 2010, *ApJ*, 717, 289
- Strong A. W., Mattox J. R., 1996, *A&A*, 308, L21
- Sturm E. et al., 2011, *Astrophys. J. Lett.*, 733, L16
- Thomas D., Greggio L., Bender R., 1998, *MNRAS*, 296, 119
- Thon R., Meusinger H., 1998, *A&A*, 338, 413
- Tremonti C. A., Heckman T. M., Kauffmann G., Brinchmann J., White S. D. M., Seibert M., Peng E. W., Schlegel D. J., 2004, *ApJ*, 613, 898
- Tremonti C. a., Moustakas J., Diamond-Stanic A. M., 2007, *ApJ*, 663, L77
- Troncoso P. et al., 2014, *A&A*, 563, A58
- Tumlinson J. et al., 2013, *ApJ*, 777, 59
- Tumlinson J. et al., 2011, *Science*, 334, 948
- Veilleux S., Cecil G., Bland-Hawthorn J., 2005, *ARA&A*, 43, 769
- Veilleux S., Osterbrock D. E., 1987, *ApJS*, 63, 295
- Vila-Costas M. B., Edmunds M. G., 1992, *MNRAS*, 259, 121
- Walter F., Brinks E., Blok W. J. G. D., Bigiel F., Kennicutt R. C., Thornley M. D., Leroy A., 2008, *AJ*, 136, 2563
- Werk J. K., Prochaska J. X., Thom C., Tumlinson J., Tripp T. M., O'Meara J. M., Peebles M. S., 2013, *ApJS*, 204, 17
- Werk J. K. et al., 2014, *ApJ*, 792, 8
- Wiersma R. P. C., Schaye J., Theuns T., 2011, *MNRAS*, 415, 353
- Yan R., Blanton M. R., 2012, *ApJ*, 747, 61
- Yoachim P., Roškar R., Debattista V. P., 2012, *ApJ*, 752, 97
- York D. G. et al., 2000, *AJ*, 120, 1579
- Zahid H. J., Dima G. I., Kewley L. J., Erb D. K., Davé R., 2012, *ApJ*, 757, 54

## APPENDIX A: ANALYTICAL SOLUTION FOR CONSTANT INFLOW MODELS

In this section we summarise the chemical evolution formalism of Peng & Maiolino (2014a) and present further exact solutions for the metallicity and total metal content.

Peng & Maiolino (2014b) models offer solutions for equations Eq. 1–4 under the following assumptions:

- (i) Constant inflow rate  $\Phi$ .
- (ii) A linear relation star formation law  $\text{SFR} = \varepsilon M_{\text{gas}}$ , with constant  $\varepsilon$ .
- (iii) Outflow rate proportional to the SFR through a constant loading factor  $\lambda$ :  $\Psi = \lambda \text{SFR}$ .

We further assume that the net nucleosynthetic yield  $y$  and return factor  $R$  are constant with time and the the inflow is of primordial gas (with zero metallicity). Under these

assumptions analytical solutions can be obtained with an explicit time dependence. As discussed in Peng & Maiolino (2014a) the equilibrium timescale

$$\tau \equiv \frac{1}{\varepsilon (1 - R + \lambda)} \quad (\text{A1})$$

is the natural timescale driving the chemical evolution of the system. For  $t \gg \tau$  physical properties of galaxies tend to their ‘equilibrium’ values. However, as discussed in Peng & Maiolino (2014a), low mass dwarf galaxies and chemically un-evolved systems will not satisfy the equilibrium condition and need to be studied in the  $t < \tau$  regime. In Table A1 we summarise the analytical solutions for a number of galaxy properties. We note that, apart from the assumptions stated above, the solutions are mathematically exact<sup>4</sup>. We also remark that, as expected, the only timescale responsible for the chemical evolution of the system is the equilibrium timescale defined above (Eq. A1).

The limits of the solutions for the equilibrium case ( $t \gg \tau$ ) have a simple physical interpretation. Star formation exactly balances out the inflow and outflow rates, the gas mass (and hence the SFR) stays constant and the stellar mass grows linearly with time. In this regime the gas phase metallicity plateaus at a constant value ( $Z_g(\text{eqm}) = y \varepsilon \tau = \frac{y}{1-R+\lambda}$ ), which depends only on the net yield, the return fraction and the outflow loading factor. Note also that the equilibrium value of the  $M_Z/M_*$  ratio is  $\frac{y}{1-R}(1 - \varepsilon \lambda \tau)$ , lower than the expected value  $M_Z/M_* = \frac{y}{1-R}$  in absence of outflows (i.e. for  $\lambda = 0$ ). The gas fraction  $f_{\text{gas}}$  can be considered as a function of  $t, \tau$  and  $\varepsilon$ , and is the best property to quantify the degree of chemical evolution of the system: systems with low gas fraction have not reached equilibrium and are chemically un-evolved, while systems with low gas fraction are in equilibrium and chemically evolved.

The analytical solutions are also an important tool to study the parameter dependences of different physical properties. In particular we can easily show that the relation between  $M_Z/M_*$  and  $f_{\text{gas}}$  depends only on the value of the outflow loading factor, and does not depend on the assumed inflow rate and star formation efficiency. In other words the position of a point in the  $f_{\text{gas}}$  vs  $M_Z/M_*$  plane depends only on  $\lambda$ . To prove this it is sufficient to observe that both  $f_{\text{gas}}$  and  $M_Z/M_*$  are only a function of  $\lambda$  and  $t/\tau$ . Therefore, eliminating  $t/\tau$ , it would be possible to write a relation between  $f_{\text{gas}}$  and  $M_Z/M_*$  which depends only on  $\lambda$ . Unfortunately the complex nature of the solutions does not allow such relation to be written in closed form. Physically this statement can be interpreted as stating that the metal deficit (i.e.  $M_Z/M_*$ ) depends only on how evolved the system is (i.e. its  $f_{\text{gas}}$ ) and the strength of its outflows (i.e.  $\lambda$ ). We note in passing that this simple result is *not* valid anymore if we assume that the inflow rate is proportional to the SFR.

Finally we note that exactly the same argument can be applied to the relation between  $f_{\text{gas}}$  and  $Z_g$ , which can therefore be shown to depend only on the outflow loading factor and not on the inflow rate and the star formation efficiency.

<sup>4</sup> The solution to the gas phase metallicity ( $Z_g$ ) presented here differs from the one in Peng & Maiolino (2014a), who solve for the metallicity evolution assuming a constant  $M_{\text{gas}}$ .

**Table A1.** Exact analytical time-dependent solution of the Peng & Maiolino (2014a) models for different galaxy properties.

Galaxy property	Exact solution	$t \ll \tau$	$t \gg \tau$
$M_g$	$\Phi \tau (1 - e^{-t/\tau})$	$\Phi t$	$\Phi \tau$
$SFR = \varepsilon M_g$	$\varepsilon \Phi \tau (1 - e^{-t/\tau})$	$\varepsilon \Phi t$	$\varepsilon \Phi \tau$
$M_\star$	$\Phi \tau^2 \varepsilon (1 - R) (t/\tau - (1 - e^{-t/\tau}))$	$\Phi \varepsilon (1 - R) t^2/2$	$\Phi \varepsilon (1 - R) \tau t$
$f_{gas} \equiv \frac{M_g}{M_g + M_\star}$	$\left[1 + \varepsilon \tau (1 - R) \left(\frac{t}{\tau} \frac{1}{1 - e^{-t/\tau}} - 1\right)\right]^{-1}$	$(1 + \varepsilon (1 - R) t/2)^{-1}$	$(1 + \varepsilon (1 - R) t)^{-1}$
$Z_g \equiv M_{Zg}/M_g$	$y \varepsilon \tau \left(1 - \frac{t/\tau e^{-t/\tau}}{1 - e^{-t/\tau}}\right)$	$y \varepsilon t/2$	$y \varepsilon \tau$
$M_Z$	$y \varepsilon \Phi \tau^2 [(1 - \varepsilon \lambda t)(t/\tau - (1 - e^{-t/\tau})) - \varepsilon \lambda t((t/\tau + 1)e^{-t/\tau} - 1)]$	$y \varepsilon \Phi t^2/2$	$y \varepsilon \Phi (1 - \varepsilon \lambda t) \tau t$
$M_Z/M_\star$	$\frac{1}{1 - R} \left[1 - \varepsilon \lambda \tau \left(1 + \frac{((1+t/\tau) e^{-t/\tau} - 1)}{t/\tau + e^{-t/\tau} - 1}\right)\right]$	$\frac{y}{1 - R}$	$\frac{y}{1 - R} (1 - \varepsilon \lambda \tau)$